Ubiquitin proteomics uncovers RNA polymerase I as a critical target of the Nse1 RING domain

Eva Ibars[1], Joan Codina-Fabra[1], Gemma Bellí[1], Celia Casas[1], Marc Tarrés[1], Roger Solé-Soler[1], Neus P. Lorite[1], Pilar Ximénez-Embún[2], Javier Muñoz[2,3], Neus Colomina[1], Jordi Torres-Rosell[1*]

[1] Departament de Ciencies Mediques Basiques, Institut de Recerca Biomedica de Lleida, Universitat de Lleida, 25198 Lleida, Spain

[2] Proteomics Unit. Spanish National Cancer Research Center (CNIO), Madrid, Spain; ProteoRed-ISCIII. Madrid, Spain

[3] Present address: Biocruces Bizkaia Health Research Institute, Barakaldo, Spain; Ikerbasque, Basque Foundation for Science. Bilbao, Spain

* Correspondence: jordi.torres@udl.cat

Lead Contact: Jordi Torres-Rosell

ABSTRACT

Ubiquitination controls numerous cellular processes, and its deregulation is associated to many pathologies. The Nse1 subunit in the Smc5/6 complex contains a RING domain with ubiquitin E3 ligase activity and essential functions in genome integrity. However, Nse1-dependent ubiquitin targets remain largely unknown. Here, we use label-free quantitative proteomics to analyse the nuclear ubiquitinome of *nse1-C274A* RING mutant cells. Our results show that Nse1 impacts on the ubiquitination of several proteins involved in DNA damage tolerance, ribosome biogenesis and metabolism that, importantly, extend beyond canonical functions of the Smc5/6 complex in chromosome disjunction. In addition, our analysis uncovers an unexpected connection between Nse1 and RNA polymerase I (RNAP I) ubiquitination. Specifically, Nse1 and the Smc5/6 complex promote the ubiquitination of K408 and K410 in the clamp domain of Rpa190, a modification that induces its degradation in response to blocks in transcriptional elongation. We propose that this mechanism contributes to Smc5/6-dependent segregation of the rDNA array, the locus transcribed by RNAP I.

INTRODUCTION

Post-translational modification of proteins is one of the most frequently used mechanisms to control protein function. These modifications can trigger conformational changes in the substrate, new interactions, or change the subcellular localization and stability of proteins. Ubiquitination can modify proteins through the formation of an isopeptide bond between the C-terminal glycine residue of ubiquitin (Ub) and the ε-amino group of a lysine in the target protein [1]. Ub itself can also be targeted for ubiquitination. To this end, it uses one of its seven lysines as acceptor sites, giving rise to a wide diversity of ubiquitin chains and possible signaling modes [1]. Depending on the type of Ub chain decoration of the substrate, ubiquitination may signal for proteasomal degradation, DNA repair, protein trafficking or extraction from a specific compartment or protein complex. Ubiquitination depends on an enzymatic cascade, involving a Ub activating enzyme (E1), a Ub conjugating enzyme (E2) and a Ub ligase enzyme (E3). In budding yeast, one E1, eleven E2s and a large family of E3 enzymes catalyze the transfer of Ub molecules to specific substrates [2]. Protein ubiquitination is balanced by ubiquitin-specific proteases (UBPs), which cleave the isopeptide bond between Ub and the target thus reversing the modification [3]. Although ubiquitination is regulated at multiple levels, E3 enzymes are strategic players, as they provide specificity to the ubiquitination reaction. Most E3s catalyze the transfer of ubiquitin by bridging the interaction between a Ub-charged E2 enzyme and the substrate. The most abundant type of E3 ligases contain RING domains, which interact with the E2 and reorient the E2-Ub thioester bond to favor the discharge of Ub onto the substrate [4]. Proper folding of RING domains requires the presence of eight conserved cysteine or histidine residues coordinating two zinc atoms in a cross-brace conformation [5]. This folding is essential for their E3 activity, and mutation of these residues severely affects ubiquitination of their targets.

Ubiquitination plays crucial roles in DNA repair, by enabling extensive signaling in response to DNA damage and replicative stress [6,7]. The maintenance of genome integrity also requires the action of the Structural Maintenance of Chromosome (SMC) complexes, present in all domains of life. SMC complexes use their ATPase activity to form loops and organize genomes during chromosome replication, segregation and DNA repair. Particularly, the Smc5/6 complex enables chromosome

disjunction by promoting removal of DNA-mediated connections between sister chromatids, which mainly arise during DNA replication and recombinational repair [8,9].

The Smc5/6 complex is assembled from eight subunits: Smc5 and Smc6, which constitute the core of the complex, and six non-SMC subunits (Nse proteins), Nse1 to Nse6. Unlike other SMC complexes, Smc5/6 contains two RING domains, located in the C-terminal part of the Nse1 and Nse2 subunits [10]. The RING domain in Nse2 has SUMO ligase activity, while the RING domain in Nse1 has Ub ligase activity [11–15]. Nse1 interacts with Nse3, a member of the highly conserved MAGE (melanoma-associated antigen) family of proteins through its N-terminal domain. The central part of Nse1 associates with Nse4, a member of the kleisin family of SMC subunits [16], to form a subcomplex that then binds to the ATPase domain of Smc5 and the neck region of Smc6. The C-terminal RING domain in Nse1 homologues (NH-RING) is characterized by the presence of a C4HC3 configuration of zinc-coordinating residues, closely related to the PHD (Plant Homology) domain and different from the conventional C3HC4 consensus found in other E3 RING domains [17]. Nse1 proteins show other features of Ub E3 ligases, including the capacity to form Ub chains in vitro [14,15]. In vitro, Nse1 ubiquitinates Nse3 and Nse4, and its E3 ligase activity is enhanced by Nse3 [14,18,19]. In human cells, Nse1 targets Mms19 in an Smc5/6-independent manner for its ubiquitination and degradation, with relevant implications in DNA polymerase function and genome stability [20]. However, and differently to Nse2, no other in vivo targets for Nse1 have been identified until now. Although the *NSE1* RING domain is not essential for viability, it contributes to the DNA repair functions of the Smc5/6 complex, and *nse1* mutant cells carrying mutations in zinc-coordinating residues show an aberrant morphology and severe growth defects, particularly under DNA damaging conditions [17,21,22].

To fill the gap in our current knowledge of Nse1-dependent Ub targets, we have compared the nuclear ubiquitinome of wild type yeast cells and *nse1* mutants bearing a C274A mutation in the RING domain [21]. Our analysis reveals that Nse1 affects the ubiquitination status of several proteins involved in ribosome biogenesis and metabolism, extending beyond canonical functions of the Smc5/6 complex in chromosome segregation. Moreover, Nse1 promotes the ubiquitination Rpa190, the

103 largest subunit in RNA Polymerase I (RNAP I), at K408 and K410, a modification
104 that promotes Rpa190 destruction. In addition, we show that this modification is
105 triggered by blocks in RNAP I elongation, including those inflicted by UV-light.
106 Overall, we propose that Rpa190 ubiquitination clears stalled RNAP I complexes
107 from rDNA chromatin to facilitate other chromosomal transactions in this locus.

RESULTS

A proteomic screen to identify Nse1-sensitive ubiquitin sites

To identify Nse1-sensitive ubiquitin sites, we profiled the ubiquitinome of wild type and *nse1-C274A* mutant cells using diGly proteomics [23]. The latter are affected in a conserved zinc-coordinating cysteine residue in the RING domain [21]. As *nse1-C274A* mutant cells are sensitive to DNA damage, and to maximize differences with their wild type counterpart, exponentially growing cultures were treated with 0.02% MMS for 1.5 hours. In addition, we fractionated whole cell extracts into soluble and nuclear fractions to reduce the complexity of the sample. Protein extracts from the nuclear fraction were trypsinized and peptides containing the signature di-glycine remnant from ubiquitin were enriched by immunopurification. Finally, ubiquitinated peptides from two biological and two technical replicates were quantified by label-free mass-spectrometry (Figure 1A)[24]. We used the flowthrough from the immunoprecipitation to quantify the total protein content in the nuclear extract, allowing the identification of 3657 proteins (Supplementary Data 1). 62 proteins were significantly less expressed (q-value<0.05) and 207 proteins were upregulated in *nse1* samples (Supplementary Figure 1B). Proteins showing higher expression in *nse1* mutant cells were enriched in functions related to purine ribonucleotide metabolism and cellular respiration (FDR 4.32E-2 and 3.90E-2). One of the proteins showing the highest expression in *nse1* mutant cells was Leu2, the auxotrophic marker used for selection of the *nse1-C274A* allele, and an internal control for the total protein quantitation (Supplementary Figure 1B). Proteins less expressed in the *nse1* mutant cells were enriched in functions related to amino acid metabolism (FDRs 2.84E-06 to 3.60E-02). In addition, three proteins encoded by 2μ plasmids (Rep1, Rep2 and Raf1) were downregulated in the *nse1-C274A* mutant, suggesting that the mutation might restrict the maintenance of episomal plasmids. Interestingly, a recent screen for mutants defective in maintenance of 2μ plasmids identified a variant in the Nse2 subunit of the Smc5/6 complex [25].

809 of the proteins in the flowthrough (around 20%) were also found after di-Gly immunoprecipitation (Figure 1B). In total, we identified 1932 ubiquitinated sites. The nuclear enrichment step used in our protocol most probably accounts for the lower

139 number of ubiquitinated peptides identified, relative to other studies [26,27]
140 (Supplementary Figure 1C). As shown in Figure 1C, 96 diGly-sites were significantly
141 (q-value<0.1) less ubiquitinated in *nse1-C274A* mutant cells, representing potential
142 Nse1-Smc5/6-dependent ubiquitin targets. Gene ontology analysis revealed that
143 peptides with lower levels of ubiquitination in *nse1-C274A* cells were enriched in
144 categories related to glycolysis, sterol synthesis, proteasome-mediated destruction,
145 ribosomal proteins and RNA polymerases (Supplementary Figure 1D). Markov
146 cluster (MCL) analysis of Nse1-dependent high confidence hits revealed the
147 presence of several subclusters, with nodes of ribosomal, glycolysis, RNA
148 polymerase, and sterol biosynthesis proteins (Figure 1D). In addition, we identified
149 one subcluster, containing DNA replication factors, which included Pol30 and
150 ribonucleotide reductase subunits.

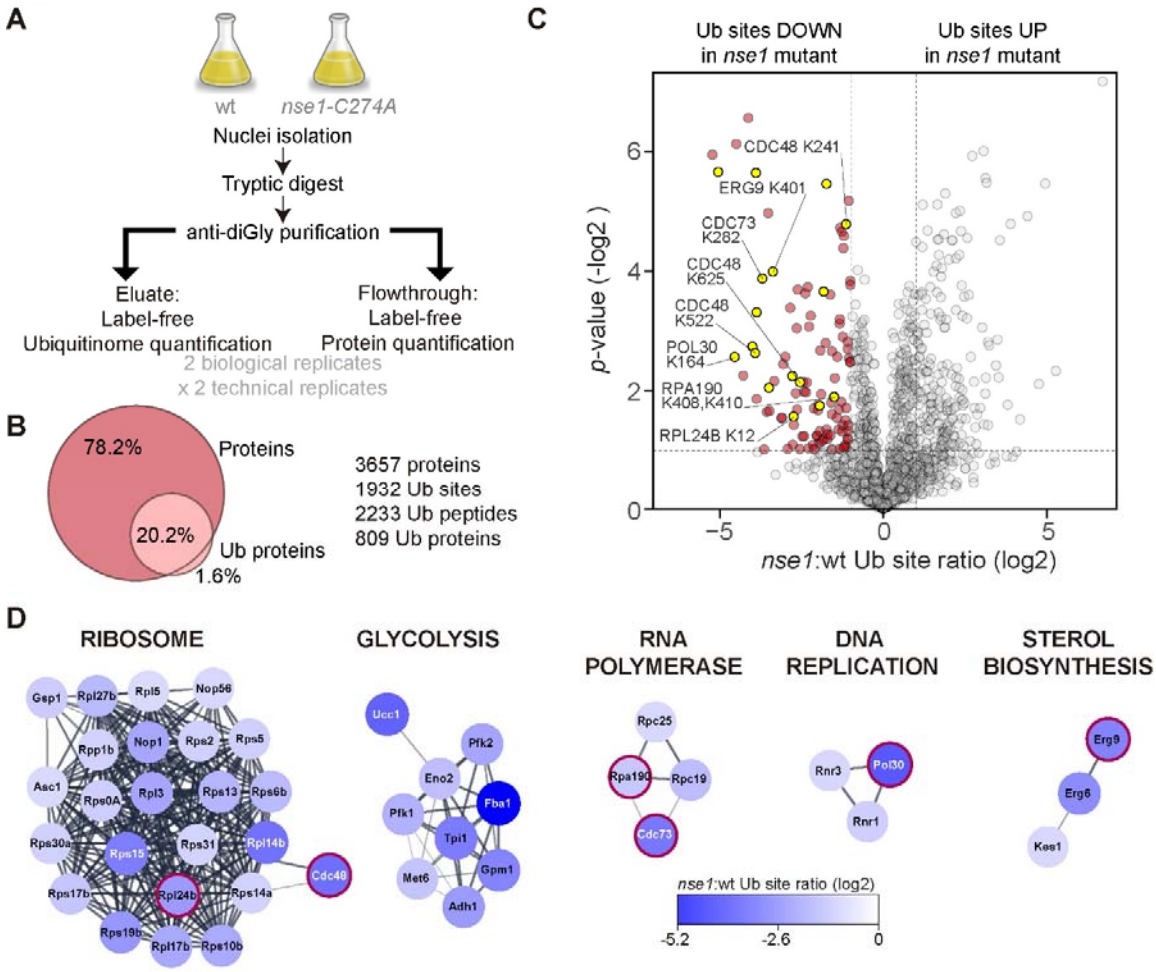

151

152 **Figure 1. A proteomic screen to identify Nse1-sensitive ubiquitin sites. A.** Experimental
153 workflow for label-free quantification of ubiquitin sites and total protein levels in nuclear fractions

form wild type and *nse1-C274A* mutant cells. Two biological and two technical replicates were used for each strain. **B**. Venn diagram of proteins identified in nuclear extract (Proteins) and in anti-diGly purification (Ub proteins) and summary of number of proteins, peptides and sites identified. **C.** Volcano plot showing the differentially ubiquitinated sites ($\log_2$ ratios) between wild type and *nse1-C274A* mutant cells on the x-axis and their statistical significance ($-\log_{10}$(*p*-value)) on the y-axis; significantly affected sites are shown above the dotted line; the ubiquitin sites downregulated in *nse1-C274A* cells are shown in red on the left side; the position of specific ubiquitination sites is shown in yellow in the graph; yellow dots without label correspond to Ub peptides from the Yhb1 protein. **D.** Cytoscape Markov cluster analysis of ubiquitin sites significantly downregulated in *nse1-C274A* cells. Note the presence of a cluster of (mainly) ribosomal proteins, proteins involved in glycolytic functions, RNA polymerase subunits, DNA replication factors and ergosterol biosynthesis enzymes. Red circles highlight targets analyzed through ubiquitin pull downs in this study.

Next, we selected seven potential Nse1-dependent ubiquitin targets from different subclusters and subjected them to further validation: Rpl24b, a 60S ribosomal subunit protein; Cdc73, a component of the Paf1 transcription elongation complex; Yhb1, a yeast flavohemoglobin involved in oxidative stress responses; Erg9, also known as squalene synthase, an enzyme that participates early in the sterol biosynthesis pathway; Cdc48, a ubiquitin-selective segregase able to extract proteins from larger cellular structures; and Pol30, a replication factor also known as sliding clamp or proliferating cell nuclear antigen (PCNA). In addition, we also confirmed Nse1-dependent ubiquitination of Rpa190 (see below). Ubiquitination of Pol30 at K164 in response to DNA damage has been extensively documented and plays important roles in genomic integrity [28]. In contrast, the role of Rpl24b, Cdc73, Yhb1, Erg9 or Cdc48 ubiquitination is unknown. Each target was tagged with a C-terminal 6xHA epitope at its endogenous location except Pol30, which was analyzed with specific antibodies. Besides, we introduced a multicopy plasmid expressing a 7xHis tagged version of ubiquitin from the *CUP1* promoter. Protein extracts from exponentially growing cells treated or not with 0,02% MMS for 1,5 hours were prepared under denaturing conditions and ubiquitinated proteins were pulled down using NiNTA beads and analyzed by western blot. As shown in Figure 2, ubiquitination of targets was either not detectable or severely impaired in *nse1-C274A* cells, relative to wild type cells, confirming our proteomic data. For Rpl24b, Cdc73 and Erg9, MMS-induced DNA damage had little effect on ubiquitination levels (Figure 2A-C). In contrast, treatment of cells with MMS upregulated the ubiquitination

188 of Yhb1, Cdc48 and, as previously known, Pol30 (Figure 2D-E). Thus, Nse1-
189 dependent ubiquitin targets do not respond similarly to DNA alkylation damage.

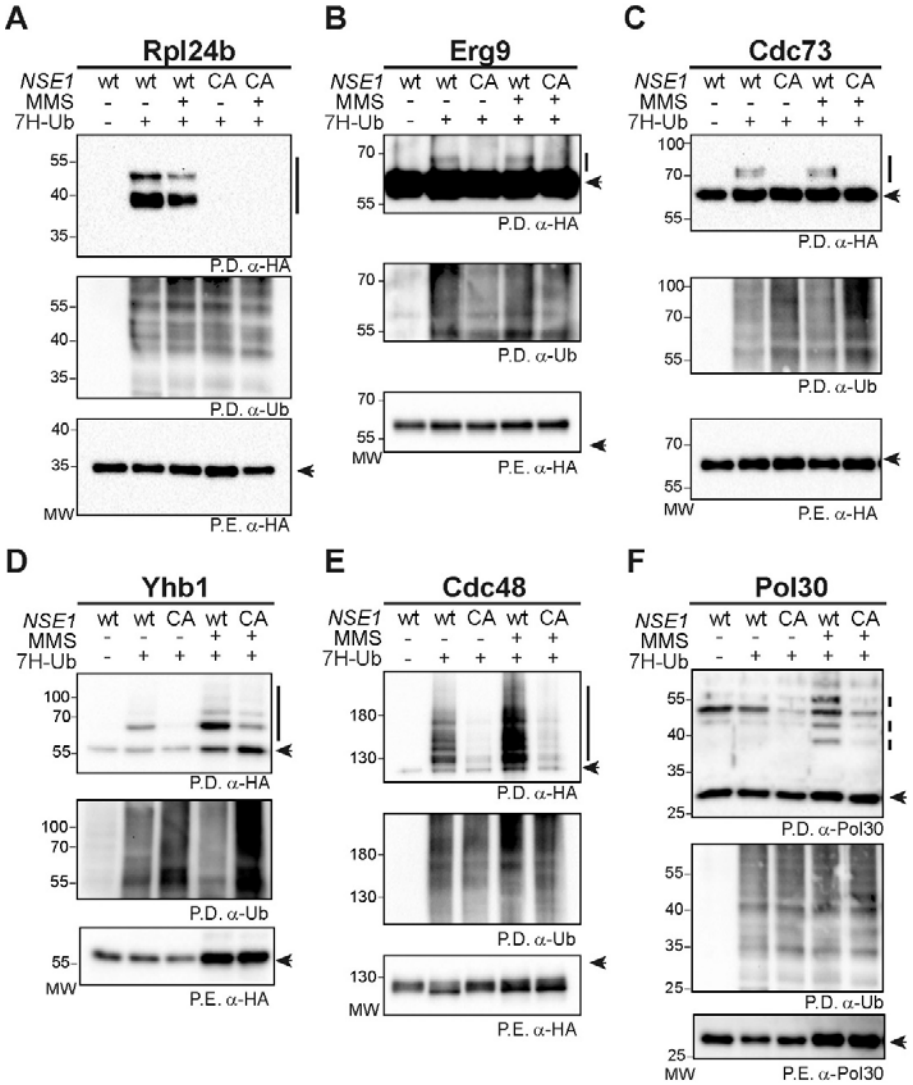

190

191 **Figure 2. Validation of Nse1-dependent ubiquitin targets.** Exponentially growing cultures of wild
192 type (wt) or *nse1-C274A* mutant (CA) cells, expressing a C-terminal 6xHA tagged version of the
193 indicated proteins from its endogenous location, and expressing (+) or not (-) a 7xHis tagged version
194 of ubiquitin (7H-Ub) from the *CUP1* promoter, were collected; where indicated, cultures were treated
195 with MMS 0.02% for 90 min before collection; ubiquitinated species from protein extracts (P.E.) were
196 analyzed by pull down (P.D.) under denaturing conditions. 6HA-tagged proteins were detected with
197 anti-HA antibodies; Pol30 was detected with a rabbit polyclonal antibody.

198 Overall, the altered ubiquitin site usage in *nse1-C274A* mutant cells indicates that
199 Nse1 participates in various cellular processes that, importantly, extend beyond
200 canonical Smc5/6 functions in chromosome replication, segregation and repair.

201 **Ubiquitination of lysine 408 and 410 modulates Rpa190 function**

202 Another group of Nse1-dependent ubiquitin targets revealed in our data comprises
203 RNA polymerase subunits. This cluster includes one subunit of RNAP I (Rpa190), a
204 subunit shared by RNAP I and III complexes (Rpc19) and an RNAP III specific
205 subunit (Rpc25). The ubiquitin site showing the greatest difference between wild type
206 and *nse1* mutants is K122 in Rpc19, followed by the double ubiquitination of K408
207 and K410 in Rpa190 (Supplementary Figure 2). Of note, Smc5/6, RNAP I and RNAP
208 III localize and operate in the rDNA array [29,30], and inactivation of RNAP I alleviates
209 the rDNA non-disjunction defects of Smc5/6 thermosensitive mutants [8]. Therefore,
210 we centered our interest in Rpa190, the largest subunit in RNAP I.

211 The K408 and K410 residues are located on top of the clamp module in the RNAP I
212 complex (Figure 3A), a region that participates in the transition between the open
213 and closed conformation of the polymerase [31,32]. Of note, sequence and structure
214 alignment of yeast Rpa190 and human Rpa194 indicate that K408 is conserved in
215 evolution and is occupied by K350 in the human RNAP I complex (Supplementary
216 Figure 3A and 3B) [33]. Rpa190 has a prominent ubiquitination band, with an
217 electrophoretic mobility equivalent to a mass increase of around 29 KDa, which
218 might reflect the addition of 3 ubiquitin molecules (Figure 3A); besides, there are two
219 extra fainter bands with a mass increase comparable to the addition of 4 and 6
220 ubiquitin molecules, respectively. To study the effect of ubiquitination at K408/K410,
221 we mutated both residues to arginine, generating an *rpa190-K408R,K410R*
222 (hereafter referred to as *rpa190-KR*) allele. This mutant was first expressed from a
223 centromeric plasmid in an *RPA190/rpa190Δ* diploid strain. Tetrad analysis of the
224 progeny showed that *rpa190-KR* mutants are viable and not affected in growth. Next,
225 we integrated the *rpa190-KR* allele and studied the ubiquitination status of the
226 mutant protein using ubiquitin pull downs. As shown in Figure 3B, Rpa190
227 ubiquitination is severely impaired in *rpa190-KR* cells, with almost no ubiquitination
228 forms detected in the western blot, indicating that ubiquitin mainly targets K408 and
229 K410 in Rpa190.

230 Rpa190 is deubiquitinated by the Ubp10 ubiquitin-specific peptidase, preventing its
231 proteasomal degradation [34]. In accordance, Rpa190 protein levels decreased in

232 *ubp10*Δ cells (Figure 3C). Remarkably, the *rpa190-KR* allele restored Rpa190
233 protein levels in *ubp10*Δ mutant cells (Figure 3C). To test if Rpa190 protein and
234 ubiquitination levels are inversely correlated, we performed ubiquitin pull downs in
235 wild type and *ubp10*Δ cells expressing *RPA190* or the *rpa190-KR* alleles from a
236 centromeric plasmid. As previously described [34], deletion of *UBP10* led to higher
237 levels of Rpa190 ubiquitination (Figure 3D), an effect that could be also directly
238 detected in protein extracts (Figure 3C). In contrast, ubiquitination was impaired in
239 the Rpa190-KR mutant protein, a situation that was more evident in *ubp10*Δ cells
240 (Figure 3D). Overall, these results demonstrate that ubiquitination at lysines K408
241 and K410 targets Rpa190 for destruction, a process that is normally counteracted
242 by the Ubp10 deubiquitinase.

243 Next, we explored situations that might promote Rpa190 ubiquitination. Rpa190
244 ubiquitination did not change in cells with high (190) or low (25) rDNA copy number
245 [35], suggesting that the relative number of actively-transcribed copies of rDNA (higher
246 in the 25 copy number strain) does not affect Rpa190 ubiquitination (Supplementary
247 Figure 4A). rDNA copy number in these strains is maintained through deletion of the
248 *FOB1* gene, which normally prevents collisions between replication and RNAP I-
249 dependent transcription, further suggesting that head-on encounters between the
250 two machineries are also not responsible for Rpa190 ubiquitination. Rpa190
251 ubiquitination did not change at different stages in the cell cycle, monitored by
252 arresting cells in G1 with alpha factor, in S phase with hydroxyurea or in G2/M with
253 nocodazole (Supplementary Figure 4B). On the other hand, MMS-induced alkylation
254 DNA damage slightly increased Rpa190 ubiquitination (Supplementary Figure 4B),
255 while irradiation of cells with UV light promoted the accumulation of ubiquitinated
256 Rpa190 species (Figure 3E and Supplementary Figure 4B), suggesting that Rpa190
257 is modified in response to bulky lesions on DNA, which are most probably
258 encountered by RNAP I during transcriptional elongation. However, UV-induced
259 ubiquitination was not accompanied by a reduction in Rpa190 protein levels (Figure
260 3E). Thus, either UV-dependent Rpa190 ubiquitination does not signal for its
261 proteasomal degradation, or only a small pool of stalled RNAP I complexes are
262 targeted by ubiquitin for destruction in response to UV damage. In addition, *rpa190-*
263 *KR* mutant cells were not sensitive to UV irradiation or alkylation DNA damage

(Supplementary Figure 4C), suggesting that Rpa190 ubiquitination might act redundantly with other mechanisms for repair of DNA lesions.

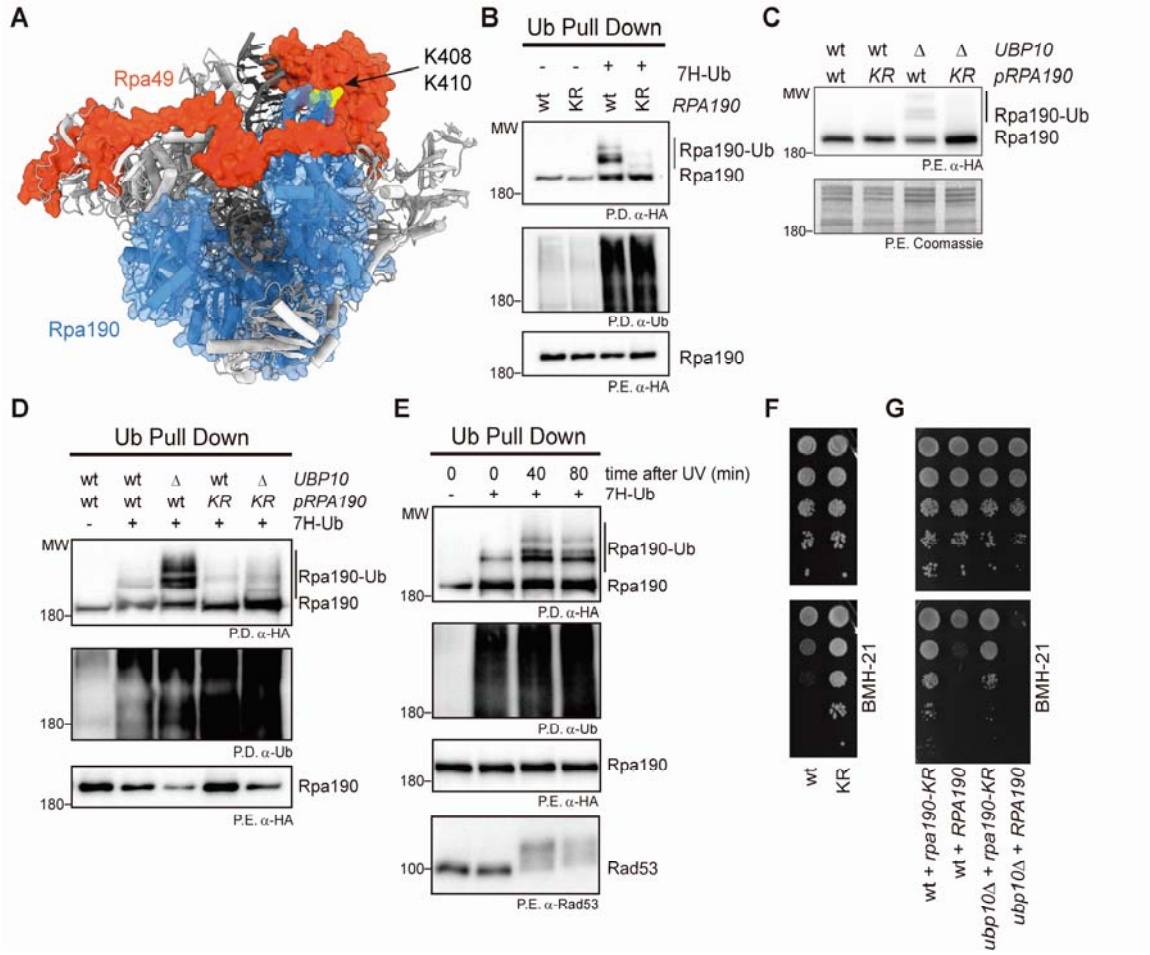

Figure 3. Ubiquitination of lysines 408 and 410, at the tip of the clamp domain, modulates Rpa190 protein levels and function. A. Structure (PDB 6H68) of an elongating Pol I complex [38]. Rpa190 is shown in blue, Rpa49 in red; K408 and K410 residues in the clamp domain are highlighted in yellow. rDNA and rRNA are shown in dark grey. **B.** Exponentially growing cultures of the indicated strains, expressing (+) or not (-) a 7xHis tagged version of ubiquitin (7H-Ub) from the *CUP1* promoter, were collected; ubiquitinated species from protein extracts (P.E.) were enriched by pull down (P.D.) of ubiquitin under denaturing conditions. **C.** Western blot analysis of wild type (wt) and *ubp10Δ* (*Δ*) mutant cells, expressing the indicated *RPA190* alleles tagged with 6xHA; wt=wild type, KR=*rpa190-KR*; bottom panel, coomassie staining of the membrane**. D.** Pull down analysis of Rpa190-6xHA ubiquitination in wild type (wt) and *ubp10Δ* (*Δ*) mutant cells expressing the indicated *RPA190* alleles; wt=wild type, KR=*rpa190-KR*; 7H-Ub=7xHis tagged ubiquitin. **E.** Ubiquitin pull down analysis in samples from an exponentially growing culture of wild type cells expressing Rpa190-6xHA, untreated or at the indicated times after UV-irradiation (300 J/m^2). UV-dependent activation of the DNA damage checkpoint was detected by the appearance of lower mobility Rad53

281 phosphorylated forms. **F**. Growth test analysis of wild type (wt) and *rpa190-KR* (KR); 10-fold serial
282 dilutions of the liquid cultures were spotted on YPD (up) or YPD with BMH-21 15 μM (bottom). **G.**
283 Wild type (wt) and *ubp10Δ* cells transformed with a centromeric vector expressing the indicated
284 *RPA190* alleles were grown overnight in selective media and spotted on YPD (up) or YPD with 15
285 μM BMH-21 (bottom); pictures were taken after 48 hours. In B, C, D and E, 6xHA-tagged Rpa190
286 was detected with anti-HA antibodies; ubiquitinated forms are indicated with a vertical bar.

287 To further explore the effects of a transcriptional elongation block on Rpa190
288 ubiquitination, we analyzed the sensitivity of *rpa190-KR* cells to BMH-21, a specific
289 inhibitor of RNAP I [36]. BMH-21 is a DNA intercalator that inhibits rRNA synthesis,
290 promoting the disassembly of the polymerase from the rDNA and the subsequent
291 degradation of Rpa190 [36,37]. Interestingly, *rpa190-KR* mutant cells were more
292 resistant to BMH-21 (Figure 3F). This phenotype was dominant, as expression of an
293 *rpa190-KR* allele from a centromeric vector in wild type cells conferred resistance to
294 BMH-21 (Figure 3G). In addition, *ubp10*Δ mutant cells were more sensitive to BMH-
295 21, as expected from their increased Rpa190 ubiquitination levels. Moreover, ectopic
296 expression of an *rpa190-KR* allele rescued the BMH-21 sensitivity of *ubp10*Δ mutant
297 cells, evidencing that K408 and K410 play a pivotal role in the response to BMH-21.
298 Overall, our findings indicate that Rpa190 ubiquitination at K408 and K410 regulates
299 RNAP I under conditions that prevent transcriptional elongation.

300 **An active Smc5/6 complex is required to sustain normal Rpa190 ubiquitination**
301 **levels**

302 To validate the decrease in Rpa190 ubiquitination in *nse1-RING* mutants, we pulled
303 down 7His-tagged ubiquitin in cells expressing a 6HA-tagged copy of Rpa190.
304 Ubiquitination levels of Rpa190 were lower in *nse1-C274A*, relative to wild type cells
305 (Figure 4A), indicating that this modification is partly dependent on the Nse1 RING
306 domain. The reduction was even more evident after treatment with MMS, conditions
307 that increased Rpa190 ubiquitination in wild type cells. In addition, the Rpa190
308 ubiquitination impairment was similar in *nse1-C274A* and *rpa190-KR* cells
309 (Supplementary Figure 5). To analyze the participation of the Smc5/6 complex in
310 Rpa190 ubiquitination, we tested various hypomorphic Smc5/6 mutants. As shown
311 in Figure 3B, *nse5-ts3* and *nse1-16*, displayed reduced Rpa190 ubiquitination levels,

312 indicating that a fully functional Smc5/6 complex is required to sustain normal
313 Rpa190 ubiquitination.

314 Monoubiquitination of Pol30 depends on Rad6, while the Ubc13-Mms2 E2 enzymes
315 stimulate its polyubiquitination. Since Pol30 ubiquitination is reduced in *nse1-C274A*
316 cells, we tested if these E2s also participate in modification of Rpa190. As shown in
317 Figure 4C, Rpa190 ubiquitination levels were lower in *rad6*Δ cells, while they were
318 not affected by the *mms2*Δ mutation, suggesting that Rad6 promotes ubiquitination
319 of Rpa190.

320 Interestingly, SUMOylation of RNAP I subunits is controlled by the Nse2 subunit in
321 the Smc5/6 complex [39]. Thus, Rpa190 SUMOylation and ubiquitination might be
322 interdependent. To analyze this possibility, we tested Rpa190 ubiquitination in
323 *nse2ΔC* mutant cells, which are severely impaired in Rpa190 SUMOylation (Figure
324 4E). Interestingly, Rpa190 ubiquitination was diminished in *nse2ΔC* mutants, relative
325 to wild type cells (Figure 4D). This suggests that perturbing RNAP I SUMOylation
326 might affect its subsequent ubiquitination; alternatively, the reduced Rpa190
327 ubiquitination might derive from deficient Smc5/6 function in *nse2ΔC* cells, as occurs
328 in *nse5-ts3* and *nse1-16* mutants (Figure 4B). In contrast, Rpa190 SUMOylation was
329 severely impaired in *rpa190-KR* cells (Figure 3E), suggesting that Rpa190
330 ubiquitination is required for its subsequent SUMOylation (Figure 4F). Of note,
331 despite the reduced SUMOylation of the Rpa190-KR protein, the pattern of SUMO
332 bands was similar to that of wild type Rpa190 (Figure 4E), suggesting that SUMO
333 may not target K408 and K410. Overall, our results indicate that Smc5/6 function is
334 required to sustain proper Rpa190 ubiquitination levels which, in turn, promotes its
335 subsequent modification with SUMO.

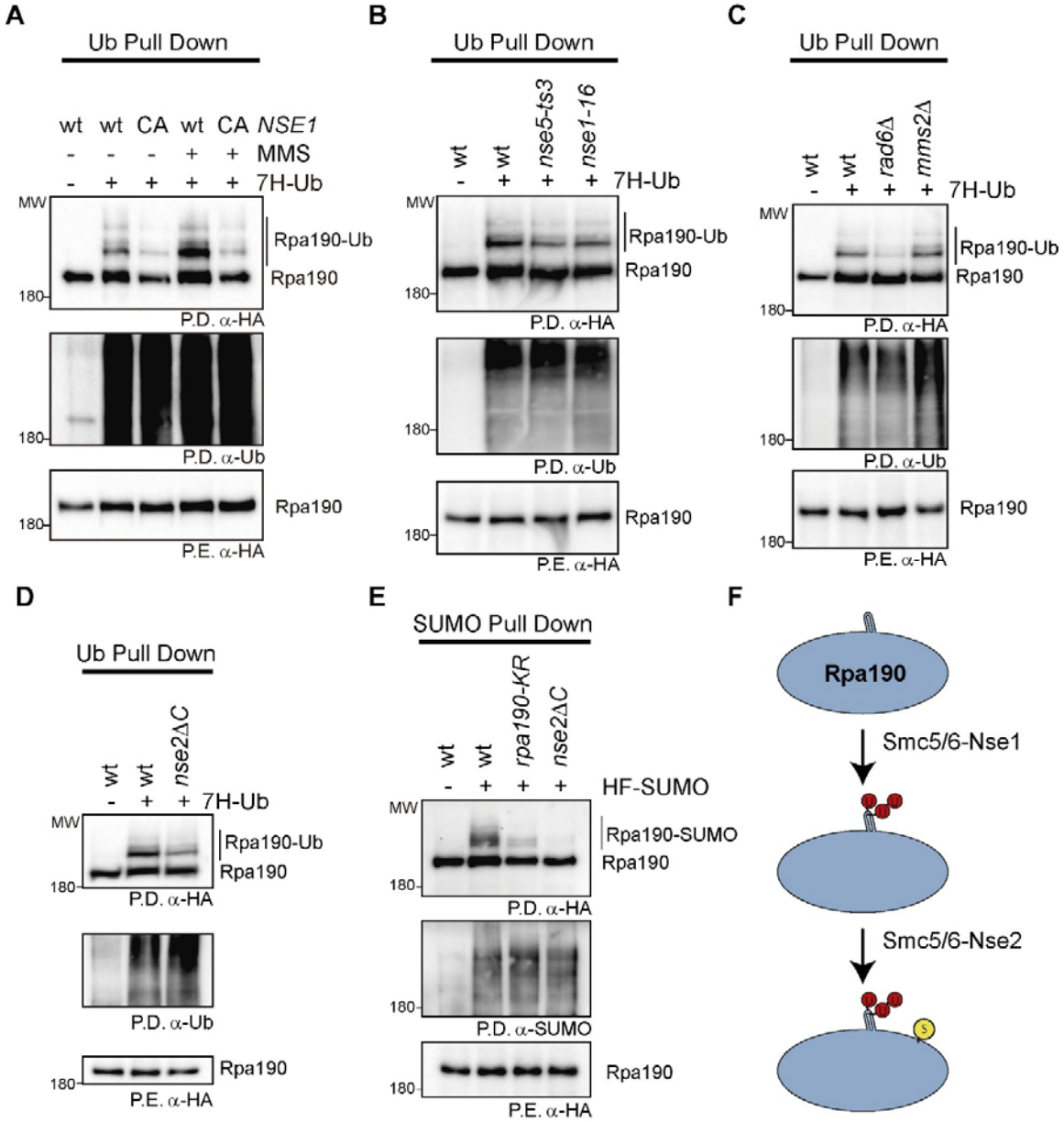

Figure 4. An active Smc5/6 complex is required to sustain normal Rpa190 ubiquitination levels. **A.** Pull down analysis of Rpa190 ubiquitination in wild type (wt) and *nse1-CA* cells; ubiquitin was pulled down (P.D.) under denaturing conditions from yeast protein extracts (P.E.) to purify ubiquitinated species. **B.** Denaturing ubiquitin pull down analysis in wild type, *nse5-ts3* and *nse1-16* cells grown at the permissive temperature (25ºC). **C.** Denaturing ubiquitin pull down analysis of Rpa190 ubiquitination in wild type and E2 (*rad6Δ* or *mms2Δ*) mutant strains. **D.** Denaturing ubiquitin pull down analysis of Rpa190 ubiquitination in wild type and *nse2ΔC* mutant strains. **E.** Denaturing SUMO pull down analysis of Rpa190 SUMOylation in *rpa190-KR* and *nse2ΔC* mutant strains. **F.** Proposed model for sequential modification of Rpa190 by Nse1-dependent ubiquitination at K408 and K410 (U, in red) followed by Nse2-dependent SUMOylation (S, in yellow). In A-E, 6xHA-tagged

347 Rpa190 was detected with anti-HA antibodies; ubiquitin or SUMO-conjugated forms of Rpa190 are
348 indicated with a vertical bar.

349 **Rpa190 ubiquitination improves rDNA segregation in *smc5/6* mutants**

350 We have previously demonstrated that RNAP I function is detrimental for rDNA
351 segregation in *smc5/6* mutants [8]. Therefore, it is possible that Smc5/6 might promote
352 local clearance of stalled RNAP I complexes through ubiquitination of the Rpa190
353 subunit, thus ensuring completion of rDNA replication and sister chromatid
354 disjunction. To test this idea, we analysed rDNA segregation, using a battery of tet
355 operators (tetO:487) inserted in the telomeric flank of the rDNA array [40]. Cultures of
356 *smc5/6* mutants cells typically fail to segregate tetO:487 in 50% of the population [29].
357 To inactivate Smc5/6 function, we used an auxin inducible degron allele of *SMC5*
358 (*smc5-aid*). After synchronization of cells in G1 with alpha factor, cultures were
359 treated with auxin to promote Smc5-aid degradation. Next, cells were released from
360 the arrest and observed under the microscope. Cells started budding at 40 minutes,
361 entered anaphase between 80 and 100 minutes, and most of them completed
362 nuclear fission 140 minutes after release from G1 (Figure 5A). Cells with two divided
363 nuclei at time points between 120 and 160 minutes were scored for segregation of
364 tetO:487 operators (Figure 5B). As shown in Figure 5C, the *rpa190-KR* allele
365 significantly aggravates the rDNA segregation defect of *smc5-aid* cells. In contrast,
366 deletion of *UBP10* had the opposite effect and improved rDNA segregation in *smc5-*
367 *aid* cells. Therefore, our results indicate that Rpa190 ubiquitination levels affect
368 rDNA segregation in *smc5-aid* mutant cells and suggest that rDNA missegregation
369 in *smc5/6* mutant cells partly stem from insufficient Rpa190 ubiquitination. Overall,
370 these observations suggest that Smc5/6-dependent ubiquitination of Rpa190 might
371 be a mechanism to dislodge stalled RNAP I complexes from chromatin, thus
372 preventing non-disjunction events in the rDNA array.

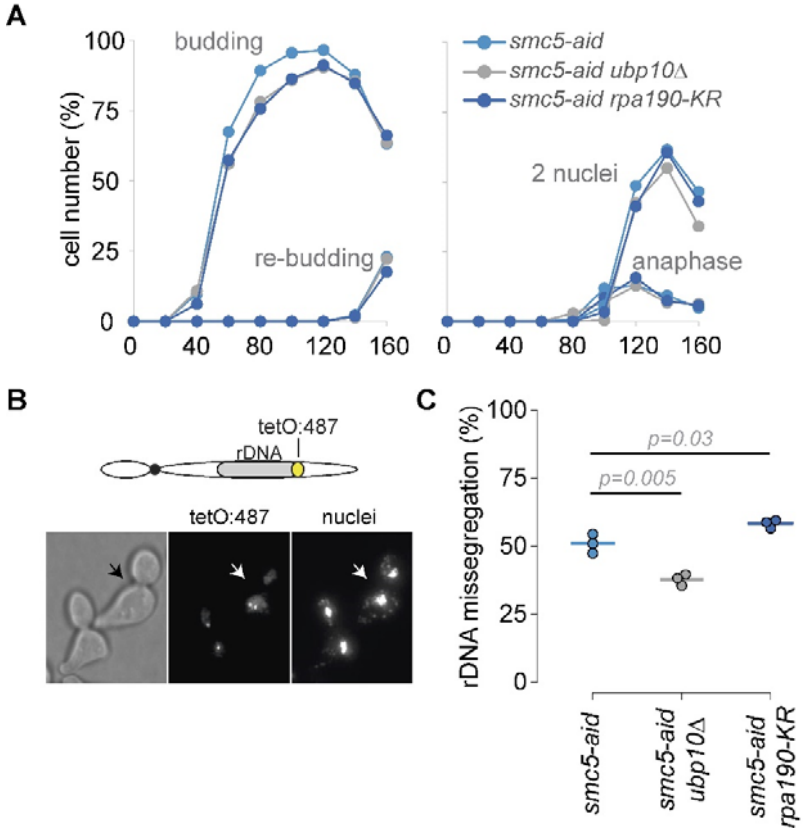

Figure 5. **Rpa190 ubiquitination improves rDNA segregation in *smc5/6* mutants. A.** Cells of the indicated genotype were synchronized in G1 with alpha factor, treated with auxin for 30 min to degrade Smc5-aid and released into a synchronous cell cycle in the presence of auxin. Samples were taken at the indicated time points for microscopic analysis and scored for budding (first S phase), re-budding (second S phase), elongated nucleus between mother and daughter cell (anaphase) and 2 nuclei (two nuclear masses between mother cell and bud). **B.** Around 50% of *smc5-aid* fail to segregate the distal part of the rDNA locus; upper panel, rDNA segregation was assayed using a battery of fluorescent *tetO* repeats inserted at the indicated position in chromosome XII; bottom panel, representative micrographs of *smc5-aid* cells at time 120 min after G1 release, nuclei stained with Hoetsch; arrow points to cell with missegregated *tetO* tags. **C.** Quantification of rDNA missegregation in cells of the indicated genotypes. Cells with two nuclei at times 105-160 min after G1 release were scored for rDNA segregation, as shown in B. Circles indicate individual measurements from 3 independent experiments; horizontal lines show medians; *p*=*p*-value, ANOVA test.

DISCUSSION

A proteomic approach to identify Nse1-dependent ubiquitin targets

The notion that inactivation of the RING domain in Nse1 impairs cell growth and sensitizes cells to DNA damage highlights its important functions in cell proliferation and genome integrity [17,21,22]. Nse1 has ubiquitin E3 ligase activity *in vitro*. This activity is enhanced by the Nse3 subunit [14]. However, the only *in vivo* substrates identified for Nse1 are (i) the Nse4 subunit of the Smc5/6 complex in yeast [19] and (ii) Mms19, a cytosolic iron-sulfur assembly (CIA) component, in humans [20]. Our label-free proteomic approach has allowed us to identify a large set of Nse1-dependent ubiquitin targets, and to reveal novel and important connections of Nse1 with DNA replication and DNA damage tolerance, ribosomal biogenesis and cell metabolism. Thus, our study should constitute a valuable source of information about the ubiquitin-dependent processes and pathways affected by the RING domain in Nse1.

Network analysis of Nse1-dependent ubiquitin targets exposes several functional clusters (Figure 1). Interestingly, a large set of proteins, including Pol I subunits, RNA processing elements and ribosomal proteins, show deregulated ubiquitination in *nse1* mutants cells, what points to ribosome biogenesis as one of the main processes controlled by Nse1. This is in accordance with the previously reported nuclear accumulation of ribosomal proteins and the ribosome biogenesis defects in *smc5/6* and *nse2Δ*RING* mutants [41], which could result from deficient controls during ribosome biogenesis. Given the relevance of ribosome biogenesis for optimal cell growth and proliferation, it is possible that the impaired fitness of *nse1* mutant cells [21,22] may be partly due to defects in ribosome synthesis and altered protein translation.

Another notable ubiquitin target identified in our proteomic screen is K164 in Pol30 (PCNA). PCNA is known to be monoubiquitinated at K164 by Rad6-Rad18 and further polyubiquitinated with K63-linked ubiquitin chains by Mms2-Ubc13-Rad5 [42,43]. In vitro, PCNA ubiquitination is very inefficient and requires prior RFC-dependent loading of PCNA onto partially heteroduplex DNA [44,45]. The requirements may be even more intricate in vivo, as PCNA ubiquitination occurs in a context of damaged and partially replicated chromatin fibers. We envisage that Smc5/6-Nse1

may coordinate sister chromatid organization and PCNA modification behind forks to enable efficient bypass of DNA lesions. In accordance, the Smc5/6 complex is recruited to damaged forks, where it aids in replisome stability and fork remodeling [46,47]. Notably, a direct link between the Smc5/6 complex and the PCNA ubiquitination machinery has been previously reported in vertebrates: Rad18 interacts with the Nse5-Nse6 homologs to recruit the Smc5/6 complex to interstrand crosslinks, a burdensome lesion that stalls replication forks [48]. However, we cannot discard the possibility that Nse1 plays an ancillary role in Pol30 ubiquitination, perhaps by reconfiguring the topology of damaged replication forks, in an unknown way, to prime full PCNA ubiquitination.

Other groups of ubiquitin targets identified in our study are related to glycolytic or sterol synthesis processes that, apparently, are not directly related to Smc5/6 or Nse1 functions on chromatin. Interestingly, some mutants in the ergosterol biosynthesis are sensitive to DNA damage, suggesting that one or more metabolite/s in this pathway could play a role in DNA damage repair [49]. On the other hand, it is worth noting that previous studies have also established a connection between the Smc5/6 complex, DNA damage and carbon metabolism [50]. Moreover, hypomorphic *NSMCE2* mutations identified in two patients have been related to a human syndrome linked to dwarfism, insulin resistance and severe metabolic abnormalities [51]. Based on our proteomic data, we propose that the Smc5/6-dependent regulation of metabolic processes may be channeled, at least partly, through protein ubiquitination.

A role for Nse1-dependent ubiquitination in Pol I transcriptional elongation

Another ubiquitin target identified in our screen is Rpa190, the large subunit of RNAP I. Based on our proteomics and pull-down experiments, we propose that ubiquitination of lysines 408 and 410 depends on Nse1. Of note, the Smc5/6 complex and RNAP I show some interesting connections. First, both of them bind to the rDNA array [29,52]; besides, RNAP I is SUMOylated in an Nse2-dependent manner [39]; in addition, inactivation of RNAP I partially relieves the rDNA missegregation phenotype of *smc5/6* mutants [8].

449 Ubiquitination levels of two Nse1-dependent ubiquitin targets identified in this study,
450 Rpa190 and Pol30, seem to be regulated by similar players, as both depend on Rad6
451 but also on the Ubp10 ubiquitin protease [34,53]. However, the outcome of the
452 modification might be different in each target: Rpa190 ubiquitination affects its
453 stability, while Pol30 ubiquitination does not. Our findings also suggest that stalling
454 of elongating RNAP I complexes by UV light damage induces Rpa190 ubiquitination.
455 In turn, Rpa190 ubiquitination can promote its degradation by the proteasome, a
456 situation that is normally counteracted by Ubp10. The analysis of double *rpa190-KR*
457 *ubp10*Δ mutants indicates that K408 and K410 are the relevant targets for ubiquitin-
458 dependent Rpa190 degradation. We speculate that cells may ubiquitinate stalled
459 RNAP I complexes to degrade them and prevent further interferences with other
460 transactions at the rDNA locus. As ongoing RNAP I complexes run into DNA
461 replication and repair processes, Nse1 dependent-ubiquitination may promote
462 RNAP I clearance from individual rDNA repeats and allow resolution of sister rDNAs.
463 In accordance, we have shown that preventing Rpa190 deubiquitination worsens
464 rDNA missegregation in Smc5/6 mutant cells, while the *rpa190-KR* mutant improves
465 it. Thus, Rpa190 ubiquitination facilitates disjunction of the rDNA array, helping to
466 maintain its integrity.

467 The localization of the ubiquitination sites in Rpa190, at the tip of the clamp domain
468 (Figure 3A), might shed clues about the role of this modification. During initiation of
469 transcription, the cleft aperture in RNAP I changes from an open conformation when
470 bound to the Rrn3 transcription factor, to a fully closed configuration in the elongating
471 complex [54,55]. In addition, the Rpa49 linker crosses on top of the cleft, passes over
472 the downstream rDNA, and binds just behind the clamp domain, acting as a safety
473 belt and securing the rDNA inside the transcribing RNAP I complex. Ubiquitination
474 sites in Rpa190 lay close to the path followed by the Rpa49 linker domain, whose
475 roles seem to be the stable clamping of the rDNA during transcriptional elongation.
476 Thus, we hypothesize that ubiquitination at the tip of the clamp might interfere with
477 Rpa49, perhaps reducing the processivity of RNAP I in preparation for its unloading
478 from the rDNA. Sequence and structure alignment indicates that lysine 350 in the
479 RPA194 subunit of the human RNAP I complex occupies the same position as lysine
480 408 in yeast (Supplementary Figure 3); moreover, quantitative diGly proteomics has

481 shown that K350 in RPA194 is also modified in vivo [23], suggesting that this
482 mechanism might be conserved in humans.

483 Although UV damage-induced Rpa190 ubiquitination is not accompanied by a global
484 reduction in Rpa190 protein levels, it is probable that Rpa190 ubiquitination occurs
485 locally, to remodel RNAP I complexes stalled by UV damage and facilitate DNA
486 repair, in an analogous way to RNAP II ubiquitination during transcription coupled
487 nucleotide excision repair (TC-NER) [56]. In accordance, RNAP I density along rDNA
488 units is altered after UV-light damage, most probably as a result of its dissociation
489 from the central and 3'-terminal side of the transcriptional unit [57]. One intriguing
490 aspect of our study is that *rpa190-KR* mutants are generally healthy and do not
491 exhibit other phenotypes in common with Smc5/6 mutants, such as sensitivity to
492 DNA damage, including lesions inflicted by UV light. However, while RNAP II
493 ubiquitin mutants are not UV sensitive, they aggravate the sensitivity of TC-NER
494 mutants [58]. Thus, onsite RNAP I ubiquitination might be used as a backup resort
495 when conventional DNA repair pathways fail. Interestingly, we have identified other
496 ubiquitin sites in RNAP I significantly under-ubiquitinated in *nse1-C274A* mutant
497 cells. For example, Rpc19, a subunit shared by RNAP I and RNAP III, showed lower
498 ubiquitination on two different sites (with 3.5 and 2.6 fold reduction) in *nse1* mutant,
499 relative to wild type. In comparison, Rpa190 ubiquitination at both K408 and K410
500 was reduced 2.8 fold in *nse1* mutant extracts. In addition, K120 in Rpa34 and K88
501 in Rpa43 were also less ubiquitinated in *nse1* mutants. Moreover, our proteomic
502 screen allowed us to identify five additional sites under-ubiquitinated in *nse1* mutant
503 cells (two sites in Rpa190 and one in Rpa135, Rpb5 and Rpb10), although
504 differences were not statistically significant, relative to the wild type. Therefore, if
505 ubiquitin redundantly targets multiple lysines in RNAP I, the modification of other
506 sites in the complex may be masking a more severe phenotype in *rpa190-*
507 *K408,410R* cells. It will be interesting to extend RNAP I KR mutations to other Nse1-
508 dependent sites, and test how it relates to Smc5/6-dependent functions.

509 Cancer cells frequently increase rRNA expression, thus making RNAP I as an
510 attractive candidate for cancer treatment [59]. Remarkably, *rpa190-KR* mutants are
511 resistant to BMH-21, a specific transcriptional elongation inhibitor of RNAP I. The
512 resistance of *rpa190-KR* cells to BMH-21 opens the question about what is the

513 nature of the problem generated by this inhibitor. BMH-21 is believed to bind G-C
514 rich areas at the rDNA and to block transcriptional elongation by RNAP I [36,37]. The
515 resistance of non-ubiquitinable *rpa190-KR* mutants suggests that the sensitivity to
516 BMH-21 is primarily due to Rpa190 ubiquitination, and not to the inability to proceed
517 with transcriptional elongation. As yeast and human cells are equipped with similar
518 tools to regulate Rpa190 ubiquitination, analysis of the physiological situations and
519 mechanisms that promote RNAP I ubiquitination in cancer cells will be of great
520 interest.

521 **METHODS**

522 **Yeast strains**

523 All strains used in this study are derivatives of EMY74.7 (*MATa his3-Δ1 leu2-3,112*
524 *trp1Δ ura3-52*), W303 (*MATa ade2-1 can1-100 his3-11,15 leu2-3,112 trp1-1 ura3-1*
525 *RAD5+*) or BY4741 (*MATa his3Δ1 leu2Δ0 met15Δ0 ura3Δ0*). A list of yeast strains
526 used in this study, together with their relevant genotype, the plasmids they carry and
527 the figure where they are used, is provided in Supplementary Tables S1 and S2.
528 Yeast cells were grown in YP (Yeast extract and Peptone) or synthetic complete
529 (SC) drop-out medium for selection of expression plasmids, plus 2% glucose. For
530 auxin-induced degrons (*smc5-aid*), IAA (SIGMA) was added to 1 mM from a 0,5 M
531 stock in water.

532 **Ubiquitinome profiling**

533 *Protein digestion*

534 To identify Nse1-dependent ubiquitin targets, we isolated the nuclear fraction from 2
535 l of wild type and *nse1-C274A* mutant yeast cells treated with MMS 0.02% for 1,5
536 hours, until reaching an OD_{600}~1.5. Cells were harvested for 5 min at 5.000 rpm,
537 resuspended and incubated for 5 min in 400 ml of azide solution (50 mM Tris-Cl-H
538 pH 7.5, azide 0.1% (15 mM)). Next, cells were centrifuged for 5 min at 5.000 rpm,
539 resuspended in 400 ml of reduction solution (500 µl of 1M Tris-HCl pH 7.5, 250 µl β-
540 ME, 49,25 ml H_2O) and incubated 30 min at room temperature. Cells were pelleted
541 and resuspended in 100 ml of SP buffer (1 M sorbitol, 20 mM phosphate buffer pH
542 7.4) and 2 mg/gr of cells of zymoliase 100T was added to each culture. Then,
543 samples were incubated at 25ºC for 20-25 min at a 100 rpm shaking agitation. After
544 checking spheroplasting, cells were sedimented at 3.200 rpm for 3 min and washed
545 with SP buffer. After removing the supernatant, spheroplasts were resuspended in
546 Ficoll buffer (18% FICOLL, 20 mM phosphate buffer pH 6.8 (PI-Roche, 1 mM EDTA,
547 5 mM chloroacetamide, 50 µM PR-619)) and kept on ice for 5 min. Samples were
548 centrifuged at 30.000 g for 20 min at 4ºC. Nuclear pellets were lysed in 10 volumes
549 of lysis buffer (5% Sodium deoxycholate, 100 mM Tris, pH 8) supplemented with
550 protease and phosphatase inhibitors (Halt, Pierce). The lysate was incubated at
551 95ºC 10 minutes and sonicated (20% intensity, 2 min, 1 sec on, 1 sec off). After

552 cooling, 1:1000 (v/v) Benzonase (Merck) was added and further incubated for 1 hour
553 at 37 C. Proteins were reduced and alkylated for 1 h with 15 mM TCEP (Sigma) and
554 30 mM CAA (Sigma) at RT in the dark. Lysates were diluted 1:5 with 50 mM Tris
555 HCl, pH 8, and proteins were digested with Lys-C (Wako) (enzyme: substrate ratio
556 1:50) for 6 h. Subsequently, samples were digested overnight at 37 °C with
557 recombinant trypsin (Trypzean, Sigma) (enzyme: substrate ratio 1:50). Enzymes
558 activity were stopped with 2% TFA (v/v). Deoxycholic acid was removed by
559 centrifugal precipitation (20 minutes at 20,000 x g). Peptides present in the
560 supernatant were desalted with 500 mg C18 SepPak SPE cartridges (Waters) and
561 lyophilized.

562 *Immunoprecipitation of di-Gly–containing peptides*

563 Enrichment of K-ε-GG peptides was performed with the PTMScan ubiquitin remnant
564 motif (K-ε-GG) kit (Cell Signaling Technology, cat. no. 5562) containing anti–K-ε-GG
565 antibody cross-linked to protein A beads. Ten milligrams of lyophilized peptides per
566 condition were gently resuspended in 1200 µl of ice cold immunoaffinity purification
567 (IAP) buffer (50 mM MOPS, pH 7.4, 10 mM Na2HPO4, and 50 mM NaCl) and
568 centrifuged at maximal speed for 5 min at 4ºC to remove insoluble materials. The
569 supernatants were mixed with 20 µl of anti–K-ε-GG of pre-conditioned antibody
570 beads and incubated for 2 h at 4°C with rotation. Samples were centrifuged and the
571 supernatant containing the unbound fraction was used to determine the total protein
572 content. Beads were washed twice with 1 ml of ice-cold IAP buffer followed by three
573 washes with ice-cold PBS and two washes with ice-cold MS-grade water. K-ε-GG
574 peptides were eluted from the antibody with 2 × 50 µl of 1% TFA. Eluted peptides
575 were desalted with C18 StageTips conditioned by washing with 80 µl of methanol
576 followed by an equilibration with 80 µl of 1% TFA. Samples were loaded on
577 StageTips, washed twice with 80 µl of 0.1% formic acid FA and eluted with 50 µl
578 60% MeCN/0.1% (FA). Eluted peptides were dried completely with vacuum
579 centrifugation and reconstituted in 0.1% FA.

580 *Mass spectrometry*

581 LC-MS/MS was carried out by coupling an Ultimate 3000 RSLCnano System
582 (Dionex) with a Q-Exactive HF-X mass spectrometer (ThermoScientific). Samples

583 were loaded into a trap column (Acclaim PepMap^{TM} 100, 100 µm x 2 cm,
584 ThermoScientific) over 3 min at a flow rate of 10 µl/min in 0.1% FA. Then peptides
585 were transferred to an analytical column (PepMap^{TM} RSLC C18, 2 µm, 75 µm x 50
586 cm, ThermoScientific). The fractions containing di-Gly-containing peptides were
587 separated using a 60 min effective linear gradient (buffer A: 0.1% FA; buffer B: 100%
588 ACN, 0.1% FA) at a flow rate of 250 nL/min. The gradient used was: 0-3 min 2% B,
589 3-5 min 6% B, 5-36 min 17.5% B, 36-60 min 25% B, 60-63 min 33% B, 63-65 min
590 45% B, 65-70 min 98% B, 70-80 min 2% B. The peptides were electrosprayed (1.9
591 kV) into the mass spectrometer through a heated capillary at 300 °C and an ion
592 funnel RF level of 40%. The mass spectrometer was operated in a data-dependent
593 mode, with an automatic switch between the MS and MS/MS scans using a top 12
594 method (minimum AGC target 8E3) and a dynamic exclusion time of 25 sec. MS
595 (350-1500 m/z) and MS/MS spectra were acquired with a resolution of 60,000 and
596 30,000 FWHM (200 m/z), respectively. Peptides were isolated using a 2 Th window
597 and fragmented using higher-energy collisional dissociation (HCD) at 27%
598 normalized collision energy. The ion target values were 3E6 for MS (25 ms maximum
599 injection time) and 1E5 for MS/MS (54 ms maximum injection time). Two
600 independent biological replicates and two technical replicates were analyzed.

601 The peptides contained in the unbound fraction were separated using a 90 min
602 effective linear gradient (buffer A: 0.1% FA; buffer B: 100% ACN, 0.1% FA) at a flow
603 rate of 250 nL/min. The gradient used was: 0-5 min 4% B, 5-7.5 min 6% B, 7.5-80
604 min 25% B, 80-94 min 42.5% B, 94-99 min 98% B, 99-105 min 2% B. The peptides
605 were electrosprayed (1.9 kV) into the mass spectrometer through a heated capillary
606 at 300 °C and an ion funnel RF level of 40%. The mass spectrometer was operated
607 in a data-dependent mode, with an automatic switch between the MS and MS/MS
608 scans using a top 12 method (minimum AGC target 8E3) and a dynamic exclusion
609 time of 40 sec. MS (350-1500 m/z) and MS/MS spectra were acquired with a
610 resolution of 60,000 and 15,000 FWHM (200 m/z), respectively. Peptides were
611 isolated using a 2 Th window and fragmented using higher-energy collisional
612 dissociation (HCD) at 27% normalized collision energy. The ion target values were
613 3E6 for MS (25 ms maximum injection time) and 1E5 for MS/MS (22 ms maximum
614 injection time). Samples were analyzed twice.

615 *Data analysis*

616 Raw files from both K-ε-GG–enriched fraction and full proteome (flow-through,
617 unbound fraction) were processed with MaxQuant (version 1.6.0.16) using the
618 standard settings against a *Saccharomyces cerevisiae* protein database
619 (UniProtKB/Swiss-Prot, 6,718 sequences) supplemented with contaminants. Label-
620 free quantification was done with match between runs (match window of 0.7 min and
621 alignment window of 20 min). Carbamidomethylation of cysteines was set as a fixed
622 modification whereas addition of glycine-glycine to lysine (only for K-ε-GG–enriched
623 fraction), methionine oxidation and N-term acetylation were variable protein
624 modifications. The minimal peptide length was set to 7 amino acids and a maximum
625 of two tryptic missed-cleavages were allowed. The results were filtered at 0.01 FDR
626 (peptide and protein level) and subsequently the "proteinGroup.txt" file and the
627 "GlyGly (K) Sites.txt" were loaded in Perseus (v1.6.0.7) for further statistical analysis.
628 The intensity of the K-ε-GG–enriched fraction was normalized by subtracting the
629 median. A minimum of 75% valid values per group was required for quantification.
630 Missing values were imputed with Perseus from the observed normal distribution of
631 intensities. Then, a two-sample Student's T-Test with a permutation-based FDR was
632 performed. Proteins with a q-value<0.05 and log_2 ratio >0.5 or < -0.5 and K-ε-GG–
633 peptides with a q-value<0.1 and log_2 ratio >1 or < -1 were considered as regulated.
634 The mass spectrometry proteomics data have been deposited to the
635 ProteomeXchange Consortium via the PRIDE partner repository with the dataset
636 identifier PXD028669.

637 **Ubiquitin and SUMO Pull downs**

638 Ubiquitin and SUMO pull-downs were done under denaturing conditions using
639 protein extracts from yeast cells carrying the *UBI* gene fused to a 7xHis tag,
640 expressed from a plasmid under the control of the *CUP1* promoter; or the *SMT3*
641 gene fused to a 6xHis-Flag epitope integrated at its endogenous location. For *UBI*
642 expression from the *CUP1* promoter, cultures were grown in SC-URA medium
643 containing $CuSO_4$ at 20 µM.

644 25 OD_{600} of exponentially growing cells (100 OD_{600} for SUMOyated Rpa190 PD)
645 were spun at 3.000 rpm 2 minutes in 50 ml tubes. Cells were then washed in cold

646 water and transferred to a 1.5 ml tube. 250 µl of Buffer A (6 M Guanidine Chloride,
647 100 mM KH_2PO_4, 10 mM Tris-HCl, 0.05% Tween-20, 15 mM imidazole, 1X protease
648 inhibitors; pH 8) and 500 µl of glass beads were added to the pellet. Cells were
649 broken using a mini-beadbeater cell disrupter (BioSpec Products) at power 6 for 1,5
650 minutes. Next, we pierced the bottom of the tube with a 21 ga. needle and set it up
651 over another 1.5 ml tube. After that, extracts were spun at 2.400 rpm to recover the
652 cell extract and discard the beads. Following, we added 700 µl of Buffer A to the
653 tube, mixed it and spun 10 minutes at 14.000 rpm at 4ºC. The supernatant was then
654 transferred to a screw cap tube, and the volume brought up to 1 ml. Finally, we added
655 70 µl of Ni-NTA (Nickel Nitrilo-triacetic Acid) agarose beads (Qiagen), and incubated
656 the mixture overnight at the orbital rotator at RT. Next, the tubes were spun at 3.400
657 rpm. The supernatant was transferred to a new tube, and the beads washed for 8
658 minutes with 900 µl of Buffer B (8 M urea, 100 mM KH_2PO_4, 10 mM Tris-HCl, 0.05%
659 Tween-20, 2 mM imidazole; pH 8). Washes were repeated a total of three times with
660 Buffer B and three times more with Buffer C (8 M urea, 100 mM KH_2PO_4, 10 mM
661 Tris-HCl, 0.05% Tween-20; pH 6.3). Finally, proteins bound to the beads were eluted
662 with 25 µl of 2xSSR (4% SDS, 250 mM Tris-HCl pH 6.8, 10% sucrose, 0.02%
663 bromophenol blue) by boiling 3 minutes at 95ºC. 30 µl of supernatants were
664 precipitated with the same volume of TCA 12% (trichloroacetic acid), washed 3 times
665 with chilled acetone, resuspended by vortexing in 30 µl of Buffer C and incubated at
666 37ºC for 20 min. Then, protein extracts (PE) were boiled with 30 µl of 2xSSR. Finally,
667 PE and PDs were centrifuged and loaded onto a SDS-PAGE for Western Blot
668 analysis.

669 **Western blot analysis**

670 This protocol was used for analysing Pol30-protein levels and modifications by
671 Western Blot. Briefly, 10 OD_{600} from an exponentially growing culture were collected
672 by centrifugation 4 minutes at 4.000 rpm and 4ºC, after adding 250 µl of TCA 20%
673 directly to the culture. The pellet was resuspended with 500 µl of TCA 20%,
674 transferred to a 1.5 ml tube and spun 6-7 seconds at high speed. Then, the
675 supernatant was removed and the pellet was resuspended again with 100 µl of TCA
676 20%. After that, we added 500 µl of glass beads and broke cells in a mini-beadbeater
677 cell disrupter (BioSpec Products) for 45 seconds. Next, the sample was transferred

678 to a new tube by making a hole with a needle at the bottom and spinning 1 minute
679 at 1.000 rpm. After that, we washed beads twice with 100 µl of TCA 5% and
680 centrifuged 10 minutes at 3.000 rpm and RT. The supernatant was discarded and
681 the pellet was resuspended with 100 µl of 1xSR (2% SDS in 0.125 M Tris-HCl pH
682 6.8) and neutralized with 50 µl of Tris-base 1 M. Samples were then boiled 3 minutes
683 at 95ºC, centrifuged 5 minutes at 13.000 rpm and protein concentration was
684 determined with the BIO-RAD Micro DC Protein Assay. Finally, 4xSS and β-
685 Mercaptoethanol were added to a volume corresponding to 30 µg of protein, loaded
686 onto an SDS-gel and analyzed by Western Blot.

687 **Generation of *rpa190-KR* mutants**

688 To obtain the *rpa190-K408,410R* allele, we mutagenized a plasmid expressing the
689 wild type gene (*pRS314-(CEN-TRP1)-RPA190*) by PCR using a pair of primers
690 containing the two point mutations and a PstI restriction site. Colonies were checked
691 by PstI digestion and sequencing. The mutant and the wild type plasmids were then
692 transformed into a diploid yeast strain with a deletion in one of the endogenous
693 copies of *RPA190*. Haploid yeast colonies carrying the *rpa190-K408,410R* plasmid
694 and a deleted chromosomal *RPA190* copy were isolated by sporulation and tetrad
695 dissection. Next, we tagged the plasmid express copy with a 6HA tag and recovered
696 the vectors from their yeast to obtain the *pRS314-(CEN-TRP1)-RPA190-*
697 *6HA:natNT2* and *pRS314-(CEN-TRP1)-rpa190-K408,410R*-6HA:natNT2 plasmids.
698 To integrate the double *KR* mutation into yeast, we used the mutant vectors as PCR
699 templates. The PCR product was transformed into yeast and colonies carrying the
700 desired mutation were selected by PstI restriction and sequencing.

701 **Gene tagging**

702 Gene tagging was performed as previously described [60], using a PCR-based method
703 for recombinational integration. A set of cassette plasmids carrying a selectable
704 marker and an epitope tag were amplified by PCR using the adequate primers to
705 direct the insertion of the cassette to the desired locus by homologous
706 recombination.

707 **Yeast growth test analysis**

708 10-fold dilution series of yeast cultures were spotted on solid medium. Plates were
709 incubated at the adequate temperature during 2-3 days and photographed with the
710 Chemiluminiscent Imager (Bio-Rad). For methyl methanesulfonate (MMS) growing
711 test analysis, MMS was added from 0.001 to 0.02% final concentrations in the YPD
712 agar media before solidification. BMH-21 (Sigma) was added to the YPD agar at a
713 15 µM concentration. Plates were incubated at 30°C until individual colonies became
714 visible in control plates.

715 **Cell Cycle experiments**

716 Exponentially growing cells were arrested in G1 by addition of 10^{-6} M alpha factor
717 (Genscript), in G2/M by addition of 15 µg/ml nocodazole (SIGMA) or 0.2 M
718 hydroxyurea (SIGMA) at 25ºC for 2 hours. In Figure 5, cultures were arrested in G1
719 by addition of 10^{-8} M alpha factor, and released by washing cells 3 times with pre-
720 warmed medium and re-suspended in media containing 0,1 mg/ml pronase E
721 (SIGMA). For microscopic visualization, DNA was stained using Hoechst at 0,5
722 µg/ml final concentration in the presence of mounting solution and 0,4% Triton X-
723 100 to permeabilize cells. For fluorescence microscopy of nuclei or tetO:487 dots,
724 series of z-focal plane images were collected with a DP30 monochrome camera
725 mounted on an upright BX51 Olympus fluorescence microscope.

726
727

728 **REFERENCES**

729 1. Komander, D. & Rape, M. The Ubiquitin Code. *Annu. Rev. Biochem.* **81**,
730 203–229 (2012).

731 2. Finley, D., Ulrich, H. D., Sommer, T. & Kaiser, P. The ubiquitin-proteasome
732 system of Saccharomyces cerevisiae. *Genetics* **192**, 319–360 (2012).

733 3. Lange, S. M., Armstrong, L. A. & Kulathu, Y. Deubiquitinases: From
734 mechanisms to their inhibition by small molecules. *Molecular Cell* **82**, 15–29
735 (2022).

736 4. Zheng, N. & Shabek, N. Ubiquitin Ligases: Structure, Function, and
737 Regulation. *Annu. Rev. Biochem.* **86**, 129–157 (2017).

738 5. Borden, K. L. B. Ring domains: Master builders of molecular scaffolds? *J.*
739 *Mol. Biol.* **297**, 1027 (2000).

740 6. Schwertman, P., Bekker-Jensen, S. & Mailand, N. Regulation of DNA
741 double-strand break repair by ubiquitin and ubiquitin-like modifiers. *Nat. Rev.*
742 *Mol. Cell Biol.* **17**, 379–394 (2016).

743 7. Mirsanaye, A. S., Typas, D. & Mailand, N. Ubiquitylation at Stressed
744 Replication Forks: Mechanisms and Functions. *Trends Cell Biol.* **31**, 584–
745 597 (2021).

746 8. Torres-Rosell, J. *et al.* Anaphase onset before complete DNA replication with
747 intact checkpoint responses. *Science (80-.).* **315**, 1411–1415 (2007).

748 9. Bermudez-Lopez, M. *et al.* The Smc5/6 complex is required for dissolution of
749 DNA-mediated sister chromatid linkages . *Nucleic Acids Res.* **38**, 6502–6512
750 (2010).

751 10. Solé-Soler, R. & Torres-Rosell, J. Smc5/6, an atypical SMC complex with
752 two RING-type subunits. *Biochemical Society Transactions* **48**, 2159–2171
753 (2020).

754 11. Zhao, X. L. & Blobel, G. A SUMO ligase is part of a nuclear multiprotein
755 complex that affects DNA repair and chromosomal organization. *Proc. Natl.*
756 *Acad. Sci. U. S. A.* **102**, 4777–4782 (2005).

757 12. Andrews, E. A. *et al.* Nse2, a component of the Smc5-6 complex, is a SUMO
758 ligase required for the response to DNA damage. *Mol. Cell. Biol.* **25**, 185–
759 196 (2005).

760 13. Potts, P. R. & Yu, H. T. Human MMS21/NSE2 is a SUMO ligase required for
761 DNA repair. *Mol. Cell. Biol.* **25**, 7021–7032 (2005).

762 14. Doyle, J. M., Gao, J., Wang, J., Yang, M. & Potts, P. R. MAGE-RING protein
763 complexes comprise a family of E3 ubiquitin ligases . *Mol. Cell* **39**, 963–974
764 (2010).

765 15. Hou, X. *et al.* Mining and characterization of ubiquitin E3 ligases expressed
766 in the mouse testis. *BMC Genomics* **13**, 495 (2012).

767 16. Palecek, J., Vidot, S., Feng, M., Doherty, A. J. & Lehmann, A. R. The Smc5-
768 Smc6 DNA repair complex - Bridging of the Smc5-Smc6 heads by the
769 kleisin, Nse4, and non-kleisin subunits. *J. Biol. Chem.* **281**, 36952–36959
770 (2006).

771 17. Pebernard, S. *et al.* Nse1 RING-like domain supports functions of the Smc5-
772 Smc6 holocomplex in genome stability. *Mol. Biol. Cell* **19**, 4099–4109 (2008).

773 18. Kozakova, L. *et al.* The melanoma-associated antigen 1 (MAGEA1) protein
774 stimulates the E3 ubiquitin-ligase activity of TRIM31 within a TRIM31-
775 MAGEA1-NSE4 complex. *Cell Cycle* **14**, 920–930 (2015).

776 19. Kolesar, P., Stejskal, K., Potesil, D., Murray, J. M. & Palecek, J. J. Role of
777 Nse1 Subunit of SMC5/6 Complex as a Ubiquitin Ligase. *Cells* **11**, (2022).

778 20. Weon, J. L., Yang, S. W. & Potts, P. R. Cytosolic Iron-Sulfur Assembly Is
779 Evolutionarily Tuned by a Cancer-Amplified Ubiquitin Ligase. *Mol. Cell* **69**,
780 113-125.e6 (2018).

781 21. Maria, S. R. S., Gangavarapu, V., Johnson, R. E., Prakash, L. & Prakash, S.
782 Requirement of Nse1, a subunit of the Smc5-Smc6 complex, for Rad52-
783 dependent postreplication repair of UV-Damaged DNA in Saccharomyces
784 cerevisiae. *Mol. Cell. Biol.* **27**, 8409–8418 (2007).

785 22. Wani, S. *et al.* Interaction of the Saccharomyces cerevisiae RING-domain
786 protein Nse1 with Nse3 and the Smc5/6 complex is required for chromosome
787 replication and stability. *Curr. Genet.* **64**, 599–617 (2018).

788 23. Kim, W. *et al.* Systematic and quantitative assessment of the ubiquitin-
789 modified proteome. *Mol. Cell* **44**, 325–40 (2011).

790 24. Lecona, E. *et al.* USP7 is a SUMO deubiquitinase essential for DNA
791 replication. *Nat. Struct. Mol. Biol.* **23**, 270–277 (2016).

792 25. Hays, M., Young, J. M., Levan, P. F. & Malik, H. S. A natural variant of the
793 essential host gene MMS21 restricts the parasitic 2-micron plasmid in
794 Saccharomyces cerevisiae. *Elife* **9**, 1–40 (2020).

795 26. Tong, Z., Kim, M. S., Pandey, A. & Espenshade, P. J. Identification of
796 candidate substrates for the golgi tul1 E3 ligase using quantitative diGly
797 proteomics in yeast. *Mol. Cell. Proteomics* **13**, 2871–2882 (2014).

798 27. Swaney, D. L. *et al.* Global analysis of phosphorylation and ubiquitylation
799 crosstalk in protein degradation. *Nat. Methods* **10**, 1–20 (2013).

800 28. Ulrich, H. D. Regulating post-translational modifications of the eukaryotic
801 replication clamp PCNA. *DNA Repair (Amst).* **8**, 461–9 (2009).

802 29. Torres-Rosell, J. *et al.* SMC5 and SMC6 genes are required for the
803 segregation of repetitive chromosome regions. *Nat. Cell Biol.* **7**, 412–419
804 (2005).

805 30. Goodfellow, S. J. & Zomerdijk, J. C. B. M. Basic mechanisms in RNA
806 polymerase I transcription of the ribosomal RNA genes. *Subcell. Biochem.*

807 **61**, 211–236 (2013).

808 31. Tafur, L. *et al.* Molecular Structures of Transcribing RNA Polymerase I. *Mol.*
809 *Cell* **64**, 1135–1143 (2016).

810 32. Neyer, S. *et al.* Structure of RNA polymerase I transcribing ribosomal DNA
811 genes. *Nature* **540**, 607–610 (2016).

812 33. Misiaszek, A. D. *et al.* Cryo-EM structures of human RNA polymerase I. *Nat.*
813 *Struct. Mol. Biol.* **28**, 997–1008 (2021).

814 34. Richardson, L. A. *et al.* A Conserved Deubiquitinating Enzyme Controls Cell
815 Growth by Regulating RNA Polymerase I Stability. *Cell Rep.* **2**, 372–385
816 (2012).

817 35. Cioci, F. *et al.* Silencing in yeast rDNA chromatin: Reciprocal relationship in
818 gene expression between RNA polymerase I and II. *Mol. Cell* **12**, 135–145
819 (2003).

820 36. Peltonen, K. *et al.* A targeting modality for destruction of RNA polymerase I
821 that possesses anticancer activity. *Cancer Cell* **25**, 77–90 (2014).

822 37. Wei, T. *et al.* Small-Molecule Targeting of RNA Polymerase I Activates a
823 Conserved Transcription Elongation Checkpoint. *Cell Rep.* **23**, 404–414
824 (2018).

825 38. Sanz-Murillo, M. *et al.* Structural basis of RNA polymerase I stalling at UV
826 light-induced DNA damage. *Proc. Natl. Acad. Sci. U. S. A.* **115**, 8972–8977
827 (2018).

828 39. Albuquerque, C. P. *et al.* Distinct SUMO ligases cooperate with Esc2 and
829 Slx5 to suppress duplication-mediated genome rearrangements. *PLoS*
830 *Genet.* **9**, e1003670 (2013).

831 40. Machín, F. *et al.* Spindle-independent condensation-mediated segregation of
832 yeast ribosomal DNA in late anaphase. *J. Cell Biol.* **168**, 209–219 (2005).

833 41. Kim, D. H. *et al.* Mms21 SUMO ligase activity promotes nucleolar function in
834 Saccharomyces cerevisiae. *Genetics* **204**, 645–658 (2016).

835 42. Hoege, C., Pfander, B., Moldovan, G. L., Pyrowolakis, G. & Jentsch, S.
836 RAD6-dependent DNA repair is linked to modification of PCNA by ubiquitin
837 and SUMO. *Nature* **419**, 135–141 (2002).

838 43. Parker, J. L. & Ulrich, H. D. Mechanistic analysis of PCNA poly-ubiquitylation
839 by the ubiquitin protein ligases Rad18 and Rad5. *EMBO J.* **28**, 3657–66
840 (2009).

841 44. Garg, P. & Burgers, P. M. Ubiquitinated proliferating cell nuclear antigen
842 activates translesion DNA polymerases eta and REV1. *Proc. Natl. Acad. Sci.*
843 *U. S. A.* **102**, 18361–6 (2005).

844 45. Haracska, L., Unk, I., Prakash, L. & Prakash, S. Ubiquitylation of yeast
845 proliferating cell nuclear antigen and its implications for translesion DNA
846 synthesis. *Proc. Natl. Acad. Sci. U. S. A.* **103**, 6477–82 (2006).

847 46. Lindroos, H. B. *et al.* Chromosomal association of the Smc5/6 complex
848 reveals that it functions in differently regulated pathways. *Mol. Cell* **22**, 755–
849 767 (2006).

850 47. Bustard, D. E. *et al.* During replication stress, non-SMC element 5 (NSE5) is
851 required for Smc5/6 protein complex functionality at stalled forks . *J. Biol.*
852 *Chem.* **287**, 11374–11383 (2012).

853 48. Räschle, M. *et al.* Proteomics reveals dynamic assembly of Repair
854 complexes during bypass of DNA cross-links. *Science (80-.).* **348**, 1253671
855 (2015).

856 49. Begley, T. J., Rosenbach, A. S., Ideker, T. & Samson, L. D. Damage
857 recovery pathways in Saccharomyces cerevisiae revealed by genomic
858 phenotyping and interactome mapping. *Mol. Cancer Res.* **1**, 103–112 (2002).

859 50. Simpson-Lavy, K. J., Bronstein, A., Kupiec, M. & Johnston, M. Cross-Talk
860 between Carbon Metabolism and the DNA Damage Response in S.
861 cerevisiae. *Cell Rep.* **12**, 1865–1875 (2015).

862 51. Payne, F. *et al.* Hypomorphism in human NSMCE2 linked to primordial
863 dwarfism and insulin resistance. *J. Clin. Invest.* **124**, 4028–4038 (2014).

864 52. Russell, J. & Zomerdijk, J. C. B. M. The RNA polymerase I transcription
865 machinery. *Biochem. Soc. Symp.* **73**, 203–216 (2006).

866 53. Gallego-Sánchez, A., Andrés, S., Conde, F., San-Segundo, P. A. & Bueno,
867 A. Reversal of PCNA ubiquitylation by Ubp10 in Saccharomyces cerevisiae.
868 *PLoS Genet.* **8**, (2012).

869 54. Fernández-Tornero, C. RNA polymerase I activation and hibernation: unique
870 mechanisms for unique genes. *Transcription* **9**, 248–254 (2018).

871 55. Engel, C., Neyer, S. & Cramer, P. Distinct Mechanisms of Transcription
872 Initiation by RNA Polymerases i and II. *Annual Review of Biophysics* **47**,
873 425–446 (2018).

874 56. Nakazawa, Y. *et al.* Ubiquitination of DNA Damage-Stalled RNAPII Promotes
875 Transcription-Coupled Repair. *Cell* **180**, 1228-1244.e24 (2020).

876 57. Tremblay, M. *et al.* UV light-induced DNA lesions cause dissociation of yeast
877 RNA polymerases-I and establishment of a specialized chromatin structure
878 at rRNA genes. *Nucleic Acids Res.* **42**, 380–395 (2014).

879 58. Somesh, B. P. *et al.* Communication between Distant Sites in RNA
880 Polymerase II through Ubiquitylation Factors and the Polymerase CTD. *Cell*
881 **129**, 57–68 (2007).

882 59. Ferreira, R., Schneekloth, J. S., Panov, K. I., Hannan, K. M. & Hannan, R. D.
883 Targeting the RNA Polymerase I Transcription for Cancer Therapy Comes of
884 Age. *Cells* **9**, (2020).

885 60. Janke, C. *et al.* A versatile toolbox for PCR-based tagging of yeast genes:
886 new fluorescent proteins, more markers and promoter substitution cassettes

887 . *Yeast* **21**, 947–962 (2004).

888

889 **AKNOWLEDGEMENTS**

890 The work in JT-R lab was supported by grants BFU2015-71308-P and PGC2018-
891 097796-B-I00 from the Ministerio de Ciencia, Innovación y Universidades, and grant
892 2017-SGR-569 from AGAUR-Generalitat de Catalunya; the IRBLLEIDA institute is
893 part of the CERCA Programme/Generalitat de Catalunya. The CNIO Proteomics Unit
894 belongs to ProteoRed, PRB3- ISCIII, supported by grant PT17/0019/0005. Eva Ibars
895 was supported by a PhD fellowship from UdL and 'Ajuts al talent en investigació
896 Biomèdica' contract from IRBLLEIDA and Diputació de Lleida. We thank Farida
897 Dakterzada for construction of yeast strains, Paul Kaufman for the polyclonal anti-
898 Pol30 antibody, Herbert Tschochner for the *pRS314-RPA190* plasmid, Rodrigo
899 Bermejo for the *YEplac195-CUP1p-7xHis-UBI* plasmid and Carlos Fernéndez-
900 Tornero and all members of the Cell Cycle lab for helpful discussions.

901 **Author contributions**

902 E.I., J.C.F., G.B., C.C., M.T., R.S-S., N.P.L., N.C. and J.T-R. performed the
903 experiments. P.X-E. and J.M. performed ubiquitin profiling. E.I., J.C.F., G.B. and J.T-
904 R. analysed and interpreted the data. J.T-R. designed the project and wrote the
905 manuscript. All authors read and approved the final version of the manuscript.

906 **Competing interests.**

907 The authors declare no competing interests.

Supplementary Figures

Supplementary Figure 1

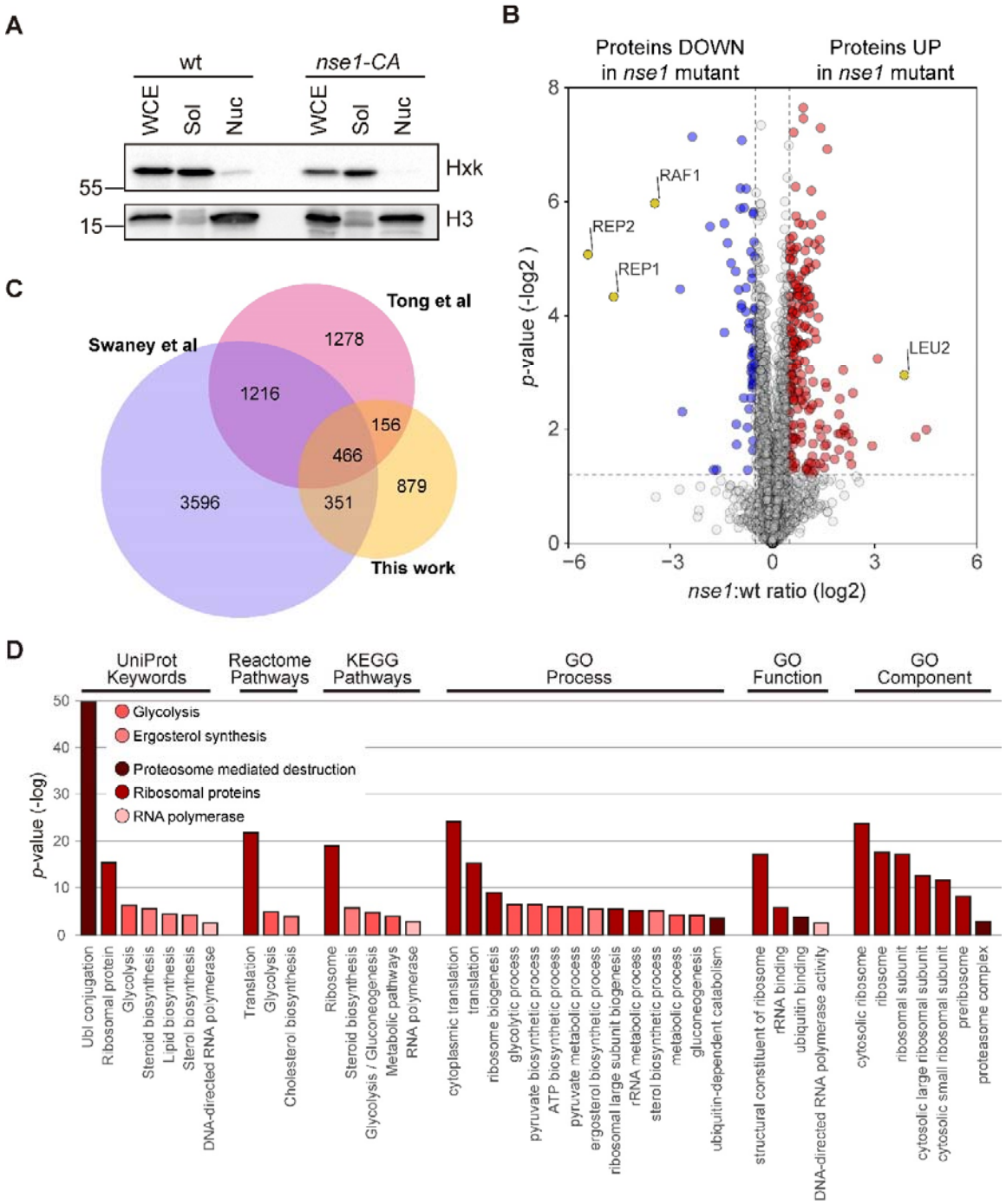

A proteomic screen to identify Nse1-sensitive ubiquitin sites. A. Fractionation of whole cell extracts (WCE) from wild type (wt) and *nse1-C274A* (*nse1-CA*) mutant yeast cells treated with MMS 0.02% into soluble cytosolic (Sol) and nuclear

(Nuc) fractions. Protein samples from WCE, Sol and Nuc were analysed by western blot and tested for the presence of hexokinase (Hxk), a soluble protein, and histone H3 (H3), a nuclear protein. **B**. Volcano plot showing the differentially expressed proteins ($\log_2$ ratios) between wild type and *nse1-C274A* mutant cells on the x-axis and their statistical significance ($-\log_{10}$(*p*-value)) on the y-axis; significantly affected proteins are shown above the dotted line; proteins down-regulated in *nse1-C274A* cells are shown in blue on the left side; proteins up-regulated in nse1-C274A cells are shown in red on the right side; the position of specific protein is shown in yellow in the graph. **C**. Venn diagram comparing ubiquitin sites identified in this work, in Swaney et al [1] and in Tong et al [2]. **D**. Gene ontology analysis of ubiquitinated sites significantly downregulated in *nse1-C274A* cells.

Supplementary Figure 2

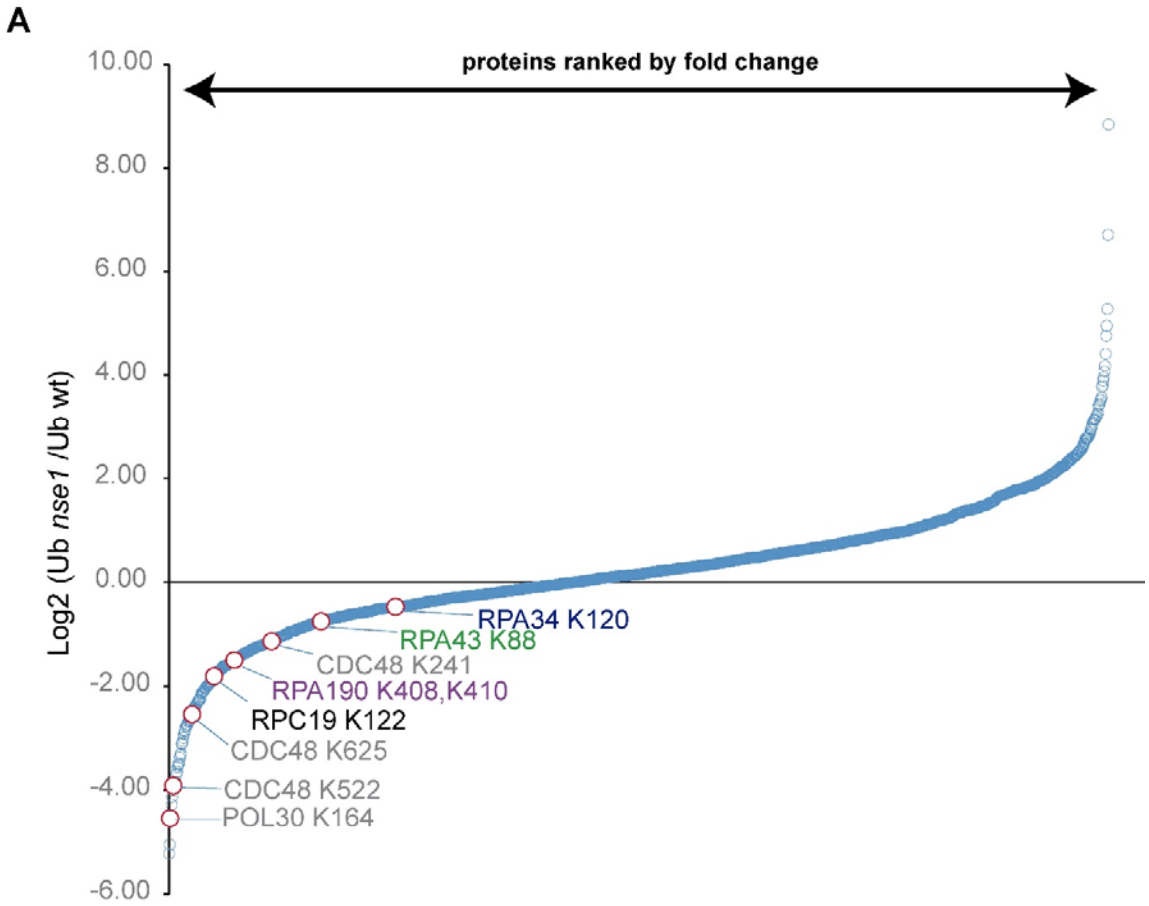

Ubiquitin sites in RNA polymerase I subunits. A. Waterfall plot showing the log2 fold change in ubiquitin site quantification from *nse1-C274A* (*nse1*) that significantly change relative to wild type (wt) nuclear extracts. Ubiquitin sites in RNAP I subunits are indicated; sites in Cdc48 and Pol30 are indicated as reference.

Supplementary Figure 3

A

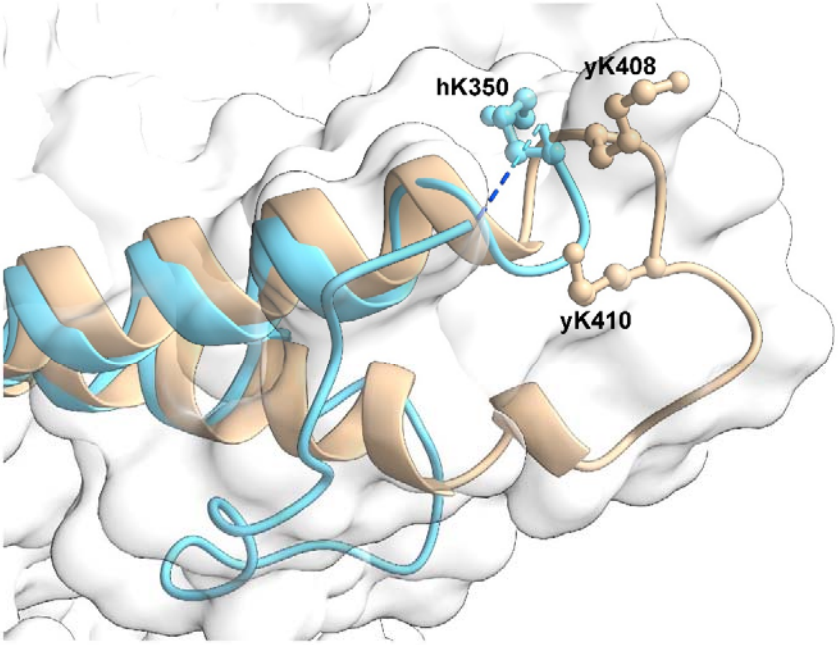

B

Structure and sequence alignment of yeast Rpa190 and human Rpa194. A. Structural alignment of clamp domains from yeast Rpa190 (in wheat; PDB 6H68 [3]) and human Rpa194 (in cyan; PDB 7OB9 [4]). The position of ubiquitinated residues, K408 and K410 in the yeast protein (yK408, yK410) and K350 in the human protein (hK350) are indicated. **B**. Sequence alignment of the clamp domain in the large subunit of the RNAP I complex. Dark blue indicates identical residues, light blue similar residues. Target lysines in the yeast protein (this study) and the human protein [5] are shown in yellow. .

Supplementary Figure 4

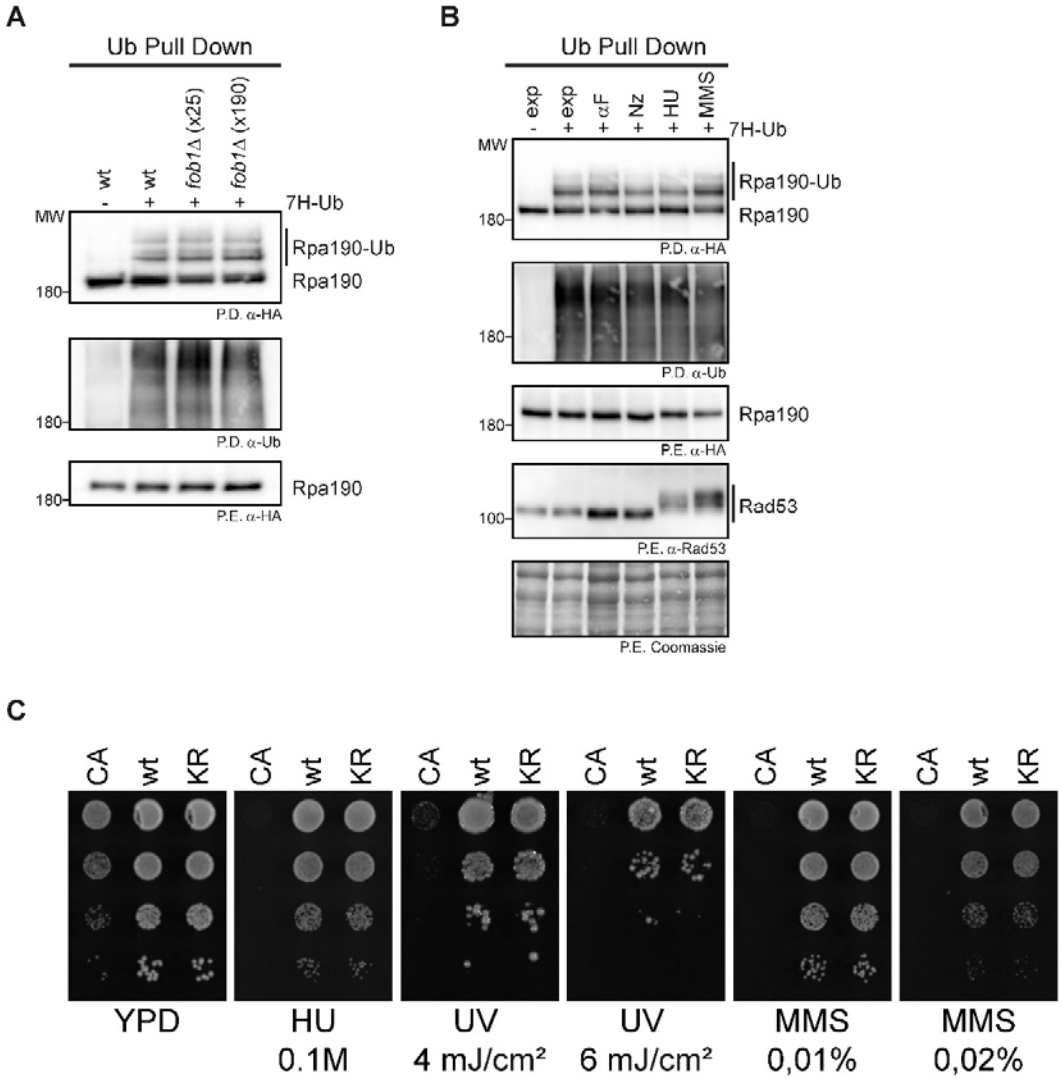

Rpa190 ubiquitination is not affected by rDNA copy number or cell cycle stage, and is not required for repair of UV-induced DNA damage. A. Exponentially growing cultures of wild type (wt), *fob1Δ* cells carrying 25 (x25) or 190 (x190) copies of the rDNA, a C-terminal 6xHA tag on *RPA190* at its endogenous location, and expressing (+) or not (-) a 7xHis tagged version of ubiquitin (7H-Ub) from the *CUP1* promoter, were collected; ubiquitinated species from protein extracts (P.E.) were pulled down (P.D.) under denaturing conditions with NiNTA beads. Rpa190-6HA species were detected with anti-HA antibodies. **B**. Exponentially (exp) growing cultures of wild type cells carrying a C-terminal 6xHA

44 tag on *RPA190*, and expressing (+) or not (-) a 7xHis tagged version of ubiquitin
45 (7H-Ub) from the *CUP1* promoter, were arrested in G1 with alpha factor (αF), in
46 G2/M with nocodazole (Nz), in S phase with hydroxyurea 0.2 M (HU) or treated
47 with MMS 0.02% to alkylate and damage DNA (MMS). Samples were processed
48 as in A for ubiquitin pull down analysis. **C**. Growth test analysis wild type (wt) and
49 *rpa190-KR* (KR) cells; 10-fold serial dilutions of the liquid cultures were spotted on
50 YPD, supplemented or not with the indicated concentrations of hydroxuyrea (HU)
51 or MMS or irradiated with the indicated doses of UV light. Plates were incubated at
52 30ºC for 3 days. The *nse1-C274A* (CA) strain was included as a control for DNA
53 damage sensitivity.

Supplementary Figure 5

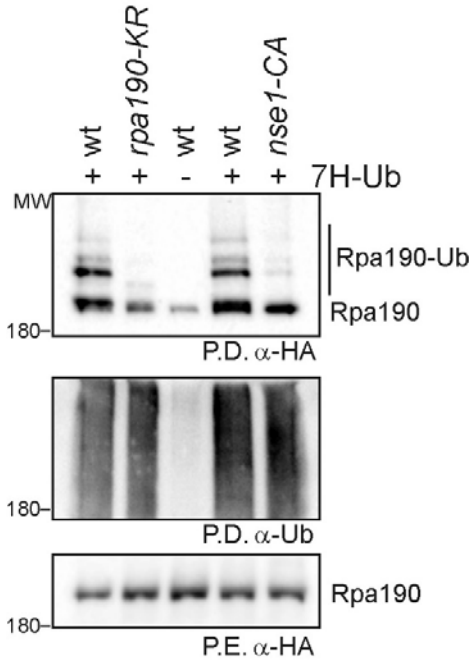

Rpa190 ubiquitination impairment is similar in *nse1-C274A* and *rpa190-KR* cells. Pull down analysis of Rpa190 ubiquitination in wild type (wt), *rpa190-KR* and *nse1-CA* cells; ubiquitin was pulled down (P.D.) under denaturing conditions from yeast protein extracts (P.E.) to purify ubiquitinated species.

60 **Supplemenetary Table 1**

NAME	GENOTYPE	PLASMIDS	FIGURE
EMY74.7	*MATa his3-Δ1 leu2-3,112 trp1Δ ura3-52*		1
YRP787	*MATa his3-Δ1 leu2-3,112 trp1Δ ura3-52 nse1::hisG pCEN-LEU2-nse1(C274A)*		1
YJC5738	*MATa his3-Δ1 leu2-3,112 trp1Δ ura3-52 RPL24B-6HA:natNT2*	p2772, p2773	2
YJC5740	*MATa his3-Δ1 leu2-3,112 trp1Δ ura3-52 nse1::hisG pCEN-LEU2-nse1(C274A) RPL24B-6HA:natNT2*	p2772, p2773	2
YJC5750	*MATa his3-Δ1 leu2-3,112 trp1Δ ura3-52 ERG9-6HA:natNT2*	p2772, p2773	2
YJC5831	*MATa his3-Δ1 leu2-3,112 trp1Δ ura3-52 nse1::hisG pCEN-LEU2-nse1(C274A) ERG9-6HA:natNT2*	p2772, p2773	2
YJC5746	*MATa his3-Δ1 leu2-3,112 trp1Δ ura3-52 CDC73-6HA:natNT2*	p2772, p2773	2
YJC5829	*MATa his3-Δ1 leu2-3,112 trp1Δ ura3-52 nse1::hisG pCEN-LEU2-nse1(C274A) CDC73-6HA:natNT2*	p2772, p2773	2
YGB5768	*MATa his3-Δ1 leu2-3,112 trp1Δ ura3-52 YHB1-6HA:HIS3MX6*	p2772, p2773	2
YGB5771	*MATa his3-Δ1 leu2-3,112 trp1Δ ura3-52 nse1::hisG pCEN-LEU2-nse1(C274A) YHB1-6HA:HIS3MX6*	p2772, p2773	2
YJC5838	*MATa his3-Δ1 leu2-3,112 trp1Δ ura3-52 CDC48-6HA:natNT2*	p2772, p2773	2
YJC5840	*MATa his3-Δ1 leu2-3,112 trp1Δ ura3-52 nse1::hisG pCEN-LEU2-nse1(C274A) CDC48-6HA:natNT2*	p2772, p2773	2
EMY74.7	*MATa his3-Δ1 leu2-3,112 trp1Δ ura3-52*	p2772, p2773	2
YRP787	*MATa his3-Δ1 leu2-3,112 trp1Δ ura3-52 nse1::hisG pCEN-LEU2-nse1(C274A)*	p2772, p2773	2
YNC2839	*MATa his3Δ1 leu2Δ0 met15Δ0 ura3Δ0 RPA190-6HA:natNT2*	p2772, p2773	3B
YEI4864	*MATa his3Δ1 leu2Δ0 met15Δ0 ura3Δ0 RPA190-K408R,K410R-6HA:natNT2*	p2772, p2773	3B
Y1838	*MATa ade2-1 can1-100 his3-11,15 leu2-3,112 trp1-1 ura3-1 RAD5+*	pEI4637, pTR5024	3C
61SC33.09	*MATa ade2-1 can1-100 his3-11 leu2-3,112 trp1-1 ura3-1 RAD5+ bar1::LEU2 ubp10::hphMX4*	pEI4637, pTR5024	3C
Y1838	*MATa ade2-1 can1-100 his3-11,15 leu2-3,112 trp1-1 ura3-1 RAD5+*	p2772, p2773, pEI4637, pTR5024	3D
61SC33.09	*MATa ade2-1 can1-100 his3-11 leu2-3,112 trp1-1 ura3-1 RAD5+ bar1::LEU2 ubp10::hphMX4*	p2773, pEI4637, pTR5024	3D
YNC2839	*MATa his3Δ1 leu2Δ0 met15Δ0 ura3Δ0 RPA190-6HA:natNT2*	p2772, p2773	3E
YNC2839	*MATa his3Δ1 leu2Δ0 met15Δ0 ura3Δ0 RPA190-6HA:natNT2*		3F
YEI4864	*MATa his3Δ1 leu2Δ0 met15Δ0 ura3Δ0 RPA190-K408R,K410R-6HA:natNT2*		3F
Y1838	*MATa ade2-1 can1-100 his3-11,15 leu2-3,112 trp1-1 ura3-1 RAD5+*	pEI4637, pTR5024	3G
61SC33.09	*MATa ade2-1 can1-100 his3-11 leu2-3,112 trp1-1 ura3-1 RAD5+ bar1::LEU2 ubp10::hphMX4*	pEI4637, pTR5024	3G
YEI3926	*MATa his3-Δ1 leu2-3,112 trp1Δ ura3-52 RPA190-6HA:kanMX4*	p2772, p2773	4A
YEI4753	*MATa his3-Δ1 leu2-3,112 trp1Δ ura3-52 nse1::hisG pCEN-LEU2-nse1(C274A) RPA190-6HA:natNT2*	p2773	4A

YNC2839	*MATa his3Δ1 leu2Δ0 met15Δ0 ura3Δ0 RPA190-6HA:natNT2*	p2772, p2773	4B
YEI4823	*nse5-ts3:kanMX4 MATa his3Δ1 leu2Δ0 ura3Δ0 met15Δ0 RPA190-6HA:natNT2*	p2773	4B
YGB5754	*nse1-16:kanMX4 MATa his3Δ1 leu2Δ0 ura3Δ0 met15Δ0 RPA190-6HA:HIS3MX6*	p2773	4B
YEI4664	*MATalpha can1Δ::MFA1pr-HIS3 lyp1Δ ura3Δ0leu2Δ0 his3Δ1 met15Δ0 RPA190-6HA:natNT2*	p2772, p2773	4C
YTR5618	*MATalpha can1Δ::MFA1pr-HIS3 lyp1Δ ura3Δ0leu2Δ0 his3Δ1 met15Δ0 RPA190-6HA:natNT2 rad6::kanMX4*	p2773	4C
YTR5620	*MATalpha can1Δ::MFA1pr-HIS3 lyp1Δ ura3Δ0leu2Δ0 his3Δ1 met15Δ0 RPA190-6HA:natNT2 mms2::kanMX4*	p2773	4C
YNC2839	*MATa his3Δ1 leu2Δ0 met15Δ0 ura3Δ0 RPA190-6HA:natNT2*	p2772, p2773	4D
YEI3959	*MATa his3Δ1 leu2Δ0 met15Δ0 ura3Δ0 RPA190-6HA:natNT2 mms21ΔC::hph*	p2773	4D
YNC2839	*MATa his3Δ1 leu2Δ0 met15Δ0 ura3Δ0 RPA190-6HA:natNT2*		4E
YSB2701	*MATa his3Δ1 leu2Δ0 met15Δ0 ura3Δ0 6HF-SMT3:kanMX6 RPA190-6HA:natNT2*		4E
YTR5776	*MATalpha can1Δ::MFA1pr-HIS3 lyp1Δ ura3Δ0leu2Δ0 his3Δ1 met15Δ0 rpa190-K408R,K410R-6HA:natNT2 6HF-SMT3:KanMX6*		4E
YSB2708	*MATa his3Δ1 leu2Δ0 met15Δ0 ura3Δ0 6HF-SMT3:kanMX6 mms21Dc::hphMX4 RPA190-6HA:natNT2*		4E
YTR1437	*Mata bar1Δ leu2-3,112 his3-Δ200 trp1-Δ63 lys2-801 pep4 ade2-1::TetR-YFP:ADE2 ChrXII(487Kb)::tetO(5.6Kb):HIS3 ura3-52::ADH1-OsTIR1-9Myc:URA3 smc5-AID:kanMX4*		5
YTR5371	*Mata bar1Δ leu2-3,112 his3-Δ200 trp1-Δ63 lys2-801 pep4 ade2-1::TetR-YFP:ADE2 ChrXII(487Kb)::tetO(5.6Kb):HIS3 ura3-52::ADH1-OsTIR1-9Myc:URA3 smc5-AID:kanMX4 ubp10::hphMX4*		5
YTR5373	*Mata bar1Δ leu2-3,112 his3-Δ200 trp1-Δ63 lys2-801 pep4 ade2-1::TetR-YFP:ADE2 ChrXII(487Kb)::tetO(5.6Kb):HIS3 ura3-52::ADH1-OsTIR1-9Myc:URA3 smc5-AID:kanMX4 rpa190-K408R,K410R-6ha:hphNT1*		5
EMY74.7	*MATa his3-Δ1 leu2-3,112 trp1Δ ura3-52*		S1A
YRP787	*MATa his3-Δ1 leu2-3,112 trp1Δ ura3-52 nse1::hisG pCEN-LEU2-nse1(C274A)*		S1A
YCC4680	*MATa leu2-3,112 ura3-1 his3-11,15 trp1-1 ade2-1 can1-100 RPA190-6HA:natNT2*		S4A
YEI3950	*MATa leu2-3,112 ura3-1 his3-11,15 trp1-1 ade2-1 can1-100 fob1::hphMX4 (rDNAx25) RPA190-6HA:kanMX*		S4A
YEI3951	*MATa leu2-3,112 ura3-1 his3-11,15 trp1-1 ade2-1 can1-100 fob1::hphMX4 (rDNAx190) RPA190-6HA:KanMX*		S4A
YNC2839	*MATa his3Δ1 leu2Δ0 met15Δ0 ura3Δ0 RPA190-6HA:natNT2*		S4B
YGB5752	*MATalpha can1Δ::MFA1pr-HIS3 lyp1Δ ura3Δ0 leu2Δ0 his3Δ1 met15Δ0 nse1-C274A:kanMX4*		S4C
Y2771	*MATalpha can1Δ::MFA1pr-HIS3 lyp1Δ ura3Δ0 leu2Δ0 his3Δ1 met15Δ0*		S4C
YEI5022	*MATalpha can1Δ::MFA1pr-HIS3 lyp1Δ ura3Δ0 leu2Δ0 his3Δ1 met15Δ0 RPA190-K408R K410R-6HA:natNT2*		S4C
YNC2839	*MATa his3Δ1 leu2Δ0 met15Δ0 ura3Δ0 RPA190-6HA:natNT2*	p2772, p2773	S5
YEI4864	*MATa his3Δ1 leu2Δ0 met15Δ0 ura3Δ0 RPA190-K408R,K410R-6HA:natNT2*	p2773	S5
YNC2839	*MATa his3Δ1 leu2Δ0 met15Δ0 ura3Δ0 RPA190-6HA:natNT2*	p2773	S5
YEI4864	*MATa his3Δ1 leu2Δ0 met15Δ0 ura3Δ0 RPA190-K408R,K410R-6HA:natNT2*	p2773	S5

Relevant genotype of yeast strains used in this study.

63 **Supplemenetary Table 2**

NAME	GENOTYPE
pEI4637	*pRS314-RPA190-K408R K410R-6HA:natNT2*
pTR5024	*pRS314-RPA190-6HA:natNT2*
p2772	*YEplac195*
p2773	*YEplac195-CUP1-HIS7-Ubi*

64 Relevant genotype of plasmids used in this study.

65 **REFERENCES**

66 1. Swaney, D. L. *et al.* Global analysis of phosphorylation and ubiquitylation
67 crosstalk in protein degradation. *Nat. Methods* **10**, 1–20 (2013).

68 2. Tong, Z., Kim, M. S., Pandey, A. & Espenshade, P. J. Identification of
69 candidate substrates for the golgi tul1 E3 ligase using quantitative diGly
70 proteomics in yeast. *Mol. Cell. Proteomics* **13**, 2871–2882 (2014).

71 3. Sanz-Murillo, M. *et al.* Structural basis of RNA polymerase I stalling at UV
72 light-induced DNA damage. *Proc. Natl. Acad. Sci. U. S. A.* **115**, 8972–8977
73 (2018).

74 4. Misiaszek, A. D. *et al.* Cryo-EM structures of human RNA polymerase I. *Nat.*
75 *Struct. Mol. Biol.* **28**, 997–1008 (2021).

76 5. Kim, W. *et al.* Systematic and quantitative assessment of the ubiquitin-
77 modified proteome. *Mol. Cell* **44**, 325–40 (2011).

78